



Effect of Modified Hydroxyapatite Nanoparticles on Sodium and Calcium Cation-Contaminated Bentonite-Water Solutions at High Temperatures

Jeffrey O. Oseh^{1,2,3,4} · M. N. A. M. Norddin^{1,2,3} · Afeez O. Gbadamosi⁵ · Issham Ismail^{1,2} · Eugene N. Ngouangna^{1,2} · Ugochukwu I. Duru⁴ · Abdul R. Risal^{1,2} · Muftahu N. Yahya^{1,2,6} · Augustine Agi⁷

Received: 27 June 2023 / Accepted: 13 September 2023 / Published online: 4 October 2023
© King Fahd University of Petroleum & Minerals 2023

Abstract

Drilling in high-temperature wells may worsen the flocculation of water-based bentonite suspension (BN-WBM), particularly when common drilling fluid contaminants like calcium cation (Ca^{2+}) and sodium cation (Na^+) are present. High concentrations of these cations can adversely affect drilling fluid rheology, filtration, and density. This can result in poor well control, pipe entrapment, poor hole cleaning, and prolonged inactivity, making drilling unprofitable. Therefore, this study examined how well CaCl_2 and NaCl work with Nano-HAp to control the viscosity and filtration of BN-WBM at 25, 120, 150, 180, and 210 °C. The salt cation's ($\text{Ca}^{2+}/\text{Na}^+$) adverse effects on BN-WBMs and Nano-HAp's salt-tolerant activities were also shown. Adding 0.5 wt% Nano-HAp reduced the BN-salt-contaminated mud viscosity, shear stress, and fluid loss at all temperatures (25–210 °C). Salt screening demonstrated that Nano-HAp adsorbed onto the BN platelets' positive edge and negative face surfaces and protected the BN ion-sensitive regions. This prevented Ca^{2+} and Na^+ from damaging the plate-like structure of the BN. When Nano-HAp is added to BN- CaCl_2 -contaminated WBM at 210 °C, the amount of fluid lost drops by 59%, from 192 to 79 mL, and the viscosity drops from 26.23 to 10.67 mPa s. In BN- NaCl -contaminated WBM, Nano-HAp reduced the viscosity from 20.82 to 8.91 mPa s and fluid loss from 169 to 73 mL by 57%. This study demonstrated that the drilling fluids performed efficiently with 0.5 wt% Nano-HAp. This study also reveals that Nano-HAp increases BN-WBM's salt and temperature resistance and efficiency in high-salinity, high-temperature settings.

Keywords Bentonite · Filtration · High temperatures · Nano-HAp · Salt contamination

Abbreviations

API	American petroleum institute
AV	Apparent viscosity
BN	Bentonite
BN/Ca	BN-calcium cation-polluted mud system

BN/HAp	BN mud system containing Nano-HAp
BN/HAp/Ca	BN-calcium cation-polluted mud system with Nano-HAp
BN/HAp/Na	BN-sodium cation-polluted mud system with Nano-HAp
BN/Na	BN-sodium cation-polluted mud system

✉ M. N. A. M. Norddin
anam@utm.my

- 1 Department of Petroleum Engineering, School of Chemical and Energy Engineering, Faculty of Engineering, Universiti Teknologi Malaysia, 81310 Johor Bahru, Malaysia
- 2 Malaysia Petroleum Resources Corporation Institute for Oil and Gas (MPRC-UTM), Universiti Teknologi Malaysia, 81310 Johor Bahru, Malaysia
- 3 Advanced Membrane Technology Research Centre (AMTEC), Nanostructured Materials Research Group (NMRG) – MD – Frontier Materials, Universiti Teknologi Malaysia, 81310 Johor Bahru, Malaysia

- 4 Department of Petroleum Engineering, School of Engineering and Engineering Technology, Federal University of Technology, P.M.B. 1526, Owerri, Imo State, Nigeria
- 5 Department of Petroleum Engineering, King Fahd University of Petroleum and Minerals, 31261 Dhahran, Saudi Arabia
- 6 Department of Chemical and Petrochemical Engineering, Bayero University, Kano, Gwarzo Road, PMB 3011, Kano, Nigeria
- 7 Faculty of Chemical and Process Engineering Technology, College of Engineering Technology, Universiti Malaysia Pahang, 26300 Gambang, Pahang, Malaysia



BN-WBM	Bentonite-polluted mud system by salt cations
Ca/P	Calcium phosphorus stoichiometric ratio
Ca ²⁺ /Na ⁺	Salt cations
CaCl ₂	Calcium chloride
CaCO ₃	Calcium carbonate
CO ₃ ²⁻	Carbonate ions
ECD	Equivalent circulating density
EDX	Energy-dispersive X-ray
FCT	Cake thickness
SEM	Scanning electron microscopy
FL	Filtrate loss
FTIR	Fourier transform infrared spectroscopy
HPHT	High-pressure and high-temperature
K_c	Cake permeability
API FCT	Cake thickness under API system
API FL	Filtrate loss under API system
Na ₂ HPO ₄	Disodium hydrogen phosphate
NaCl	Sodium chloride
Nano-HAp	SDS-aided hydroxyapatite nanoparticles
NPs	Nanoparticles
OBM	Oil-based drilling muds
OH ⁻	Hydroxyl ions
PO ₄ ³⁻	Phosphate ions
PSD	Size distribution of particles
q_r	Filtration rate
SDS	Sodium dodecyl sulphate
SO ₄ ⁻	Sulphate ions
TEM	Transmission electron microscopy
TGA	Thermal gravimetric analysis
WBM	Water-based drilling mud
XRD	X-ray diffraction pattern
μ	Apparent viscosity
τ	Shear stress

1 Introduction

Recent discoveries of major oil and gas fields are mostly in deep and ultra-deep formations. The development of deep and ultra-deep oil and gas resources will be one of the primary paths in the future oil industry [1]. This is due to the fast expansion of deep and ultra-deep fields and rising global demand for oil and gas commodities [1]. Deep and ultra-deep formations include high pressure and high temperature (HPHT) and complicated geological conditions (mainly salt gypsum layers) [2], making drilling mud performance and maintenance more demanding. Thus, selecting the right drilling mud system is crucial for safety and efficiency of drilling operation.

The use of water-based muds (WBMs) rather than oil-based muds (OBMs) has become increasingly significant for drilling oil and gas wells due to environmental concerns and the cost of treating drilling mud waste. However, conventional WBMs formulated using bentonites (BN) and polymers (natural or synthetic) fail at complicated geological features of deep and ultra-deep wells, such as HPHT, high stress, and high salt content [2, 3]. High temperatures and salt concentrations in deep and ultra-deep wells cause drilling mud treatment agents to cross-link and degrade [4, 5]. WBM failures can cause wellbore safety mishap like well blowout, pipe sticking, hole pack-off, bit failure, leakages, and formation damage, which increase drilling costs, damage oil and gas reservoirs, and hinder deep oil and gas development [5, 6]. Therefore, safe and economical drilling requires consistent drilling fluid properties, such as density, viscosity, yield point, gel strength, and fluid loss volume [4].

Inorganic salts, such as calcium chloride (CaCl₂) and sodium chloride (NaCl), from intricate geological formations like saltwater, cement, limestone, and gypsum beds can harm drilling mud properties and impair their efficacy [7, 8]. Salt contaminants primarily originate from gypsum beds deep inside oil fields subsea, where hydratable cations (Ca²⁺ and Na⁺) can invade gypsum beds deep within oil fields up to 40,000 mg/L (4 wt%) [8, 9]. Also, in offshore operations, saltwater is used to prepare drilling muds, or hydratable salts are added to the drilling mud system to create a salt-saturated WBM [8, 9]. Deep and ultra-deep wells are more likely to meet salt beds or salt gypsum layers, which may contaminate water-based bentonite solutions (BN-WBMs). BN particle-charged surfaces are susceptible to salt cations while drilling salt beds [3, 5]. When BN-WBMs are pumped into the wellbore via gypsum beds, electrostatic attraction causes Ca²⁺ and/or Na⁺ cations to adhere to the negatively charged BN surface [10]. This action compresses the BN particle's diffusion double layer, creating a charge discrepancy in the electrical double layer and forming aggregated and flocculated BN structures that drastically alter drilling mud characteristics [8–10].

By swelling and dispersing, BN particles in freshwater increase water viscosity and restrict fluid loss to the formation by forming a thin filter cake with low-permeability [8, 11]. BN particle aggregation and flocculation impair rheology and filtration control under CaCl₂ or NaCl conditions at high temperatures [6, 8]. Also, desorption between polymers and BN will become easier, which reduces the protective colloid ability of polymers and disperses BN particles [9, 11]. Thus, drilling mud rheology must be closely monitored and controlled to avert higher equivalent circulating density and pressure leakage. Also, to maintain wellbore stability, drilling mud must minimize surge pressure and increase pipe tripping [2, 10]. Wellbore stability and reservoir protection depend on

filtration management [10, 12]. Therefore, developing high-salt and high-temperature WBM systems is crucial for safe, economical, and efficient deep and ultra-deep well drilling.

Over the years, high-temperature and high-salt-resistant polymeric additives for WBMs have been developed enough to deal with high salt cations and high temperatures in deep and ultra-deep formations [13, 14]. However, these high-temperature salt-resistant polymeric additives cannot withstand deep and ultra-deep well drillings when faced with high salinity ($\geq 100,000$ mg/L) and high temperatures (≥ 200 °C) [15]. Therefore, the birth of nanoparticles (NPs) is seen as a possible solution for addressing some of the aforementioned issues and increasing profitability in different applications, specifically in drilling operations. This is due to their good stability at high temperatures [5], efficient bond networks [16], and high salt resistance characteristics [5, 7]. Compared to BN and polymers, the salt cation and temperature resistance characteristics of NPs can facilitate and improve drilling in deep and deeper wells. This is because NPs reduce the polymer chains mobility and oxidation under high-temperature conditions and increase the polymers' resilience to high temperatures and high salt contents [2, 17]. Also, in salt-contaminated WBMs, NPs protect the BN layers from salt cation attack and significantly control the viscosity and fluid loss volume of the salty drilling fluids [17]. Thus, the cation-NP combinations lead to changing the net charges in the BN-water suspension, stabilizing the BN layers to decrease salt cation effects [5]. Due to the adverse effects of salt contaminants on drilling efficiency, the aforementioned studies and others presented in Table 1 have been designed as anti-salt drilling fluids for improved drilling operations [18–28].

In recent years, the increasing use of NPs or nanoscale materials, such as hydroxyapatite (HAp), has increased the importance of nanotechnology in the field of bioceramics. HAp is a natural mineral type of calcium-phosphate apatite with the chemical formula $\text{Ca}_{10}(\text{PO}_4)_6(\text{OH})_2$ to represent the crystal unit cell of two entities [29–31]. HAp is the same mineral found in bones and teeth, and it is predominantly composed of calcium and phosphate in a 1.67:1 ratio (1.664 ± 0.005) [29, 31]. HAp is particularly biocompatible with the human body because it has a structure comparable to the mineral in bone [30]. It is bioactive, non-toxic, and inexpensive to produce [32]. Furthermore, HAp has excellent mechanical stability, a high surface energy and aspect ratio, high fracture toughness, and an adjustable surface [31, 33]. It also has a built-in sufficient functional group (OH^- , PO_4^{3-} , and CO_3^{2-}) that allows for easy surface modification to control its particle size and improve fluid dispersion [30, 33]. It also has outstanding thermal resistance that can withstand 600 °C without deterioration [16, 31]. Moreover, the efficiency of Nano-HAp, like that of other NPs, is dependent on its preparation, modification, and surface properties [16, 33].

In aqueous conditions, precipitation of chemicals in situ from calcium and phosphorus sources produces particles of Nano-HAp that have a propensity to aggregate [16, 34, 35]. The dispersion of Nano-HAp in drilling fluids may deteriorate with time due to aggregation. Also, the chemical stability of NPs is important to prevent aggregation and sedimentation, which are two critical phenomena affecting the stability of nano-based drilling fluids [16, 29]. Agglomerated drilling muds increase particle size, decrease the stability of particles and efficiency, and make drilling operations unprofitable [36]. Anionic sodium dodecyl sulphate (SDS) is a popular particle-modification surfactant [33, 37]. SDS-surface-modified HAp increases surface properties, particle dispersion, and fluid stability with no or few agglomerations [16, 33, 38]. Thus, Nano-HAp particle surfaces could be modified in situ with SDS to improve their characteristics and performance in drilling mud systems.

Recent applications of Nano-HAp in drilling fluids show that it improved the rheological and filtration control properties of the base fluid [39]. In enhanced oil recovery, it has also promotes nanofluids and reduces reservoir rock adsorption for improved oil recovery [16]. In high and ultra-high-temperature environments, high salt cations often contaminate WBMs. Thus, when designing and analysing WBM properties with NPs, salt contamination ought to be taken into account. Furthermore, significant progress has been made in developing salt-resistant WBMs with NPs in deep and ultra-deep well drillings [2, 18, 21], but the potential of NPs in BN-water solutions under salt cation assault at high temperatures requires further investigation. In one of the recent studies conducted by the authors [39], an insight into the fluid properties of the Nano-HAp-based drilling muds showed the capability of the Nano-HAp particles to improve the base fluid properties and function as an anti-salt contaminant additive at 25 and 120 °C. Moreover, reviews of different studies show that examination of drilling fluid properties and performance under calcium and sodium cations contamination at higher temperatures is limited, requiring more investigations with either existing additives or new additives. Consequently, this research utilizes the advantageous fluid properties of Nano-HAp to further explore its behaviour when subjected to salt cation assault within the high-temperature range of 150–210 °C. It also provides more understanding of the mechanism behind the screening of Ca^{2+} and Na^+ ions from BN platelets in BN-WBMs.

Hence, the objective of this study is to improve the high-temperature performance of BN-WBMs under high CaCl_2 and NaCl concentrations between 25 and 210 °C using SDS-supported particles of Nano-HAp. For this purpose, an SDS-supported Nano-HAp was synthesized through an in situ chemical precipitation technique and characterized by zeta potential magnitude, particle size distribution (PSD), thermogravimetric analysis (TGA), transmission electron

Table 1 An overview of some previous studies on different anti-salt additives for improving drilling fluid properties at different test conditions

Salts	Concentrations	Drilling muds	Test conditions	Results summary	Authors
NaCl, CaCl ₂ , and MgCl ₂	0.5, 1, and 2 wt% Fe ₃ O ₄ NPs	BN-based WBMs	25 °C and 100 psi	Fe ₃ O ₄ NPs enhance WBDF rheology in both salt-free and salty environments, with better performance in the former	[18]
NaCl and CaCl ₂	5% of Adaptive plugging agent (ADS)	ADS-based WBMs	25 °C and 180 °C and 100 psi	ADS can withstand temperatures up to 180 °C, NaCl salt saturation, and CaCl ₂ up to 5%	[19]
CaCl ₂	4% Amphoteric polymer ADD and 4% anionic polymer (AD)	4% BN in BN-WBMs	25 °C and 100 psi and 150 °C ageing for 16 h	ADD had more viscosity and shear stress than AD. ADD controlled fluid loss better than AD under 11.1% CaCl ₂ contamination and 150 °C hot rolling	[20]
CaCl ₂ and NaCl	4 wt% CaCl ₂ and NaCl added in 0.5 wt% functionalized cellulose nanocrystals (fCNCs)	4 wt% of BN in BN-WBMs	25 °C and 100 psi	Ca ²⁺ produced a higher fluid loss than Na ⁺ . At 4 wt% CaCl ₂ , 0.5 wt% fCNCs in BN-WBMs decreased API FL, FCT, filtration rate, and cake permeability by 69.3, 47.1, 65.3, and 81.2%, respectively	[21]
CaCl ₂ and NaCl	0.5–3 wt% of Modified XG XG-g-AAA	XG-g-AAA-based WBMs	25, 120, 150, 180, and 200 °C. and 100 psi and 100 psi and ageing for 16 h	XG-g-AAA was highly contaminant-tolerant and compatible. It resists 2 wt% CaCl ₂ and 35 wt% NaCl at ambient temperature and 0.75% and 5% after 150 °C ageing	[22]
CaCl ₂	0.5, 1, 1.5, 2, 2.5, and 3 wt% ionic liquid additive (PASV)	4.0 wt% BN and 11 wt% for all PASV/BN-WBMs	25 and 120 °C. 100 psi and 250 psi. 1.5–3 wt% of PASV at 80–150 °C	BN-WBMs with 3.0% of PASV effectively controlled Ca ²⁺ -contaminated fluid loss and could withstand up to 70 wt% Ca ²⁺ , approaching saturation at 25 °C	[23]
NaCl	3 wt% of NaCl and 10 wt% of BN	20,000 ppm of CMC and 4000 ppm of Temperature resistance PASM-t	30, 80, and 150 °C. 100 psi and 250 psi. 12 h ageing at 150 °C. 1.5–3 wt% of PASV at 80–150 °C	Results demonstrated that PASM's aqueous solution had a greater viscosity in NaCl and at higher temperatures than CMC and blank drilling fluid	[24]

Table 1 (continued)

Salts	Concentrations	Drilling muds	Test conditions	Results summary	Authors
NaCl	5 and 36 wt% of NaCl. 4 wt% BN, and 0.5, 1, 1.5, and 2 wt% of NS-ANAD	Nano-silica-modified co-polymer (NS-ANAD) gel and	25, 150, 180, and 200 °C ageing for 16 h and 100 psi	Even after ageing at 200 °C and saturated salt conditions, 2.0 wt% NS-ANAD co-polymer gels showed excellent filtration and fluid properties	[25]
NaCl and KCl	3%, 5% and 7% KCl and NaCl	WBM	234, 288, 342, 396, and 450 °F. Between 15,000 and 35,000 psi	NaCl-contaminated samples exhibited greater shear stress curves than WBM, whereas KCl-contaminated samples had lower ones	[26]
NaCl	0.24 lbm/gal NaCl, 0.25 lbm/gal BN, 0.02 and 0.05 lbm/gal of xanthan gum, and 0.02 lbm/gal diutan gum	BN-WBM containing diutan gum and xanthan gum (XC)	100 psi, 25 °C, 100 °C, and 120 °C ageing of drilling muds for 16 h	BN-WBM containing XC and diutan gum caused less formation damage and was tolerant of contamination with Na ⁺ cations. XC/diutan gum in BN-WBM after ageing at 25 °C, 100 °C, and 120 °C for 16 h reduced the fluid loss by 16%, 19%, and 34%, respectively	[27]
MgCl ₂	1 and 1.5 wt% of MgCl ₂	MgCl ₂ added to Lignite and Gypsum drilling muds	86, 100, and 200 °F	MgCl ₂ decreases drilling mud fluid loss. MgCl ₂ salt concentration increases formation fluid loss. Gypsum mud may survive higher temperatures than 5 wt% MgCl ₂ lignite mud, which failed at 200 °F	[28]

microscopy (TEM), Fourier transform infrared spectroscopy (FTIR), electron-dispersive X-ray (EDX), and X-ray diffraction (XRD) analysis. The rheology and filtrate loss features of BN-WBMs with SDS-supported particles of Nano-HAp at selected temperatures (25–210 °C) and Ca²⁺/Na⁺ cation assault were comprehensively investigated.

The basic principle of this research is to elucidate the underlying processes by which salt cations adversely affect BN-WBMs and to show the efficacy of Nano-HAp as a salt-inhibiting agent in drilling fluids. The rational use of in situ SDS-surface treatment of Nano-HAp enabled this process. The Nano-HAp particles, which have been treated with SDS, attach to the BN platelets on both their edge and face surfaces. This attachment successfully protects the ion-sensitive regions of the platelets. As a result, there is a discernible

improvement in the resistance of the BN-WBMs to salt contaminants. Zeta potential analysis of the different samples of drilling fluid taken at 25 and 210 °C and SEM analysis of the surface morphology of the filter cake that formed at 210 °C helped confirm the improvement in properties of BN-WBM containing Nano-HAp. The originality of this study centres on all the fluid properties examined at 150, 180, and 210 °C, the filter cake surface morphological analysis by SEM, and the investigation of the stability of the drilling muds through zeta potential measurements. The point of these measurements at higher temperatures and in the presence of salt cations is to find out if SDS-treated Nano-HAp can be used in high-temperature wells and salty environments. These investigations were not conducted in the earlier



study by the authors using the designed Nano-HAp particles [39].

2 Experimental Details

BN-WBMs were made in the laboratory using methods allowed by API RP 13B-2 [40], and their filtration and rheological features were measured at 25 °C (before ageing) and at 120 °C after ageing for 16 h according to API RP 13B-1 [41]. To highlight drilling in deep and ultra-deep water formations, often characterized by high temperatures and salt contents, selected temperatures of 150, 180, and 210 °C were applied to study the rheological and filtration behaviours of the particles of Nano-HAp in BN-WBMs under salt cation assault.

2.1 Test Items

SDS (Mol. Wt. = 288.38 g/mol, density = 1.01 g/cm³), calcium carbonate (CaCO₃) (Mol. Wt. = 100.09 g/mol, density = 2.71 g/cm³), disodium hydrogen phosphate (Na₂HPO₄) (Mol. Wt. = 141.96 g/mol, density = 1.70 g/cm³), NaCl, sodium BN, CaCl₂, and sodium hydroxide (NaOH) were acquired from QR&C, Japan.

2.2 Procedures

2.2.1 In Situ Synthesis of SDS-Supported Particles of Nano-HAp

Figure 1 depicts an in situ chemical precipitation synthesis technique for Nano-HAp with SDS template acting as a modifier and synthesis control agent according to previous procedures [31, 33], while the creation process of the particles of Nano-HAp assisted by SDS is shown in Fig. 2. Following Fig. 1, Na₂HPO₄ of 68.1 g was mixed very slowly in 100 mL of water and stirred at a temperature of 80 °C at 600 rpm for 30 min. CaCO₃ of 80.1 g was gradually added into the mixture using a graduated burette to ensure effective dissolving while continuously mixing at 600 rpm. The SDS molecules can chelate and attract Ca²⁺ ions from CaCO₃ solution to form SiO₄⁻-O-Ca²⁺-O-SiO₄⁻ bonds. The nucleation of HAp crystals occurs when PO₄³⁻ ions interact with the SiO₄⁻-O-Ca²⁺-O-SiO₄⁻ [30, 33]. To reduce calcite production in the precipitates, calcium was added to the phosphate drop-wise. SDS solution of 200 mL dissolved in water of 300 mL using 10 g SDS was introduced into the solution as it stirs after controlling the pH level of the mixture to 10 obtained by using NaOH of 0.625 M. A solution pH (10) greater than pH of 9 prevents a small amount of calcium from forming in the end product's (Nano-HAp) structure [31].

The mixture was then constantly agitated to produce a suspension at 600 rpm and cooled naturally under atmospheric air conditions to avoid thermal shock on the formed precipitates. The formed precipitates were separated using Eppendorf centrifuge 5810R at room temperature for 20 min at 6000 rpm and rinsed three times with distilled water to eliminate any impurities. The sample was dried in an oven for 24 h at 60 °C to eliminate all water molecules and volatile compounds, cooled naturally, pulverized, and stored for characterization and as a fluid additive.

2.2.2 Characterization of SDS-Supported Nano-HAp

The dispersion of NPs in drilling fluids may deteriorate with time due to aggregation. The electrical stability of SDS and Nano-HAp particles dissolved in water was measured using the Malvern Ultra Zetasizer, United Kingdom for long-term dispersion stability in the drilling fluids system. The pH was set between 2 and 12, and NaOH and HCl isoelectric titrations of 0.5 M each were adopted. The temperature utilized was constant at 25 °C. PSD analysis was carried out using a disposable-size cuvette and a 4 attenuator on a particle size analyser (PSA, Malvern Instruments, UK). Data from a Perkin-Elmer FTIR 2000 spectrophotometer were gathered at 25 °C over 16 scans between 400 and 4000 cm⁻¹, with a resolution of 4 cm⁻¹, to get information on the functional groups and bonds of Nano-HAp. With EDX analysis, the Nano-HAp elemental composition was also evaluated. The temperature resistance of Nano-HAp particles was investigated in a nitrogen-containing atmosphere using a DTG/TGA instrument, Q5000 Version, USA, heated at a rate of 10 °C/min between 20 and 1000 °C.

X-ray diffraction patterns were used to determine the phase composition of Nano-HAp powder. In an ethanol medium, 1.0 g of the powder was manually ground using an agate mortar and pestle. This is done to reduce powder loss during grinding and to limit structural damage to the powder phases induced by grinding. The diffraction patterns were captured using a Bruker AXS D8 Advance, a Cu K α radiation source of $\lambda = 1.5418 \text{ \AA}$, a graphite monochromator, and a Ni filter. Anode voltage, 40 kV; tube current, 40 mA; 2θ angular range, 20°–60°; scan step, 0.02°; scan rate, 0.01 s/step; slit, 0.6 mm; and energy discriminator, 0.20–0.26 keV, were used in the measurement, as described in a recent work [33]. The spectra were analysed using MDI JADE 5.0 software using a worldwide database of standard XRD peaks of hydroxyapatite (ICDD 9–0432). The size distribution and morphology of particles of Nano-HAp were determined using a 120 kV high-resolution TEM method (HT7700 Hitachi, Japan).



Fig. 1 The preparation technique of the particles of Nano-HAp

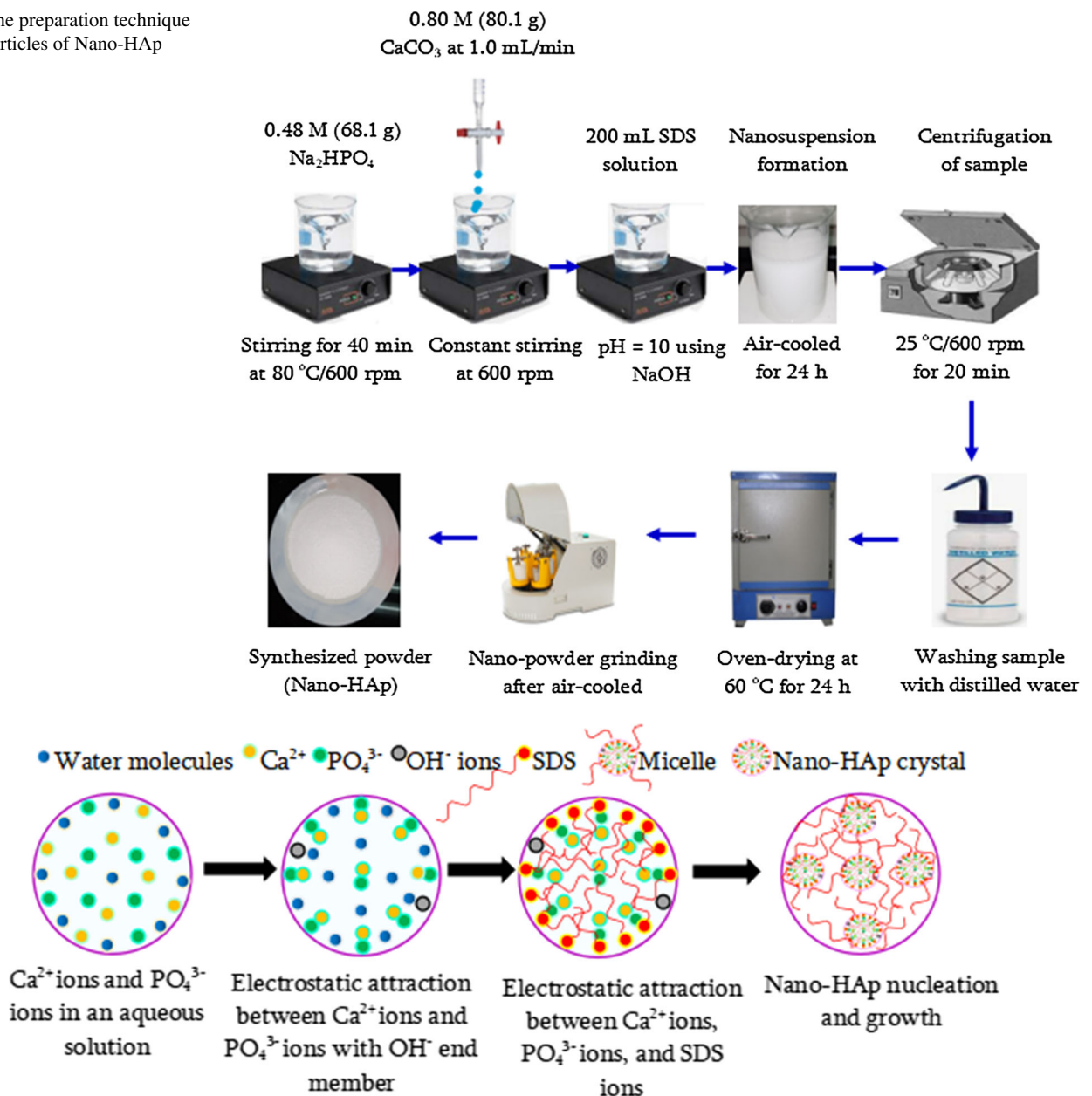


Fig. 2 Creation process of the particles of Nano-HAp in the presence of SDS surfactant

2.3 Preparation of Different Mud Systems Under Salt Cations Assault

The properties of drilling mud, such as viscosity, fluid loss, and density, can be impaired by salt cation contamination, such as Na⁺ or Ca²⁺ [21]. These salts can alter the hydration, performance, flocculation, and dispersion characteristics of the particles of drilling mud, particularly BN clay, rendering it incapable of transporting and suspending cuttings [21]. As a result, it was determined in this study whether Nano-HAp in BN-WBMs could withstand the assault of Ca²⁺ and Na⁺ cations at high temperatures. In this study, a total of

30 drilling mud samples (sample size) were formulated for six sets of drilling muds, and they are BN, BN/Na, BN/Ca, BN/HAp, BN/HAp/Na, and BN/HAp/Ca. For each set of drilling mud formulated, five mud samples of the same composition were formulated for five temperatures of 25, 120, 150, 180, and 210 °C (i.e. 1 sample each for a given temperature). For each given temperature and mud sample, all the investigated parameters were measured twice for consistency, and the average values for each measured parameter were recorded. The test BN-WBMs was prepared by first weighing the correct amount of BN on a high precision scale (precision of ± 0.01 g). Each set of drilling mud formulated

followed the recommended standard, which is adding a 1.0 g weight concentration of material to a 350-mL laboratory barrel, which is equivalent to 1 pound of material added to 1 bbl of the actual drilling mud system.

Following this, the various drilling mud formulations are as follows: First, in a cylindrical container of 1000 mL, 4.8 wt% BN was mixed with 350 mL of deionized water (test conditions: 9.0 pH, 25 °C water temperature, and 210 mg/L salinity) to form BN-WBM. The BN-WBM mud system was then modified by adding NaCl at a concentration of 5 wt.%; the resulting mixture is known as BN/Na. The CaCl₂ mud system, giving it the name BN/Ca, was developed using the same concentration and procedure as the NaCl mud system. To create the Nano-HAp drilling mud system (BN/HAp), 0.5 wt% was added to the BN mud. To evaluate Nano-HAp's salt resistance, a concentration of 5 wt% of each of NaCl and CaCl₂ was introduced into the formulated BN/HAp mud system to make BN/HAp/Na and BN/HAp/Ca drilling mud systems, respectively. Each set of drilling mud was mechanically agitated for 60 min at 10,000 tr/min. The formulated drilling muds were aged in a Fann roller oven (Model 704ET, USA) for 16 h at temperatures of 120, 150, 180, and 210 °C.

A low concentration of Nano-HAp of 0.5 wt% was used to determine its resistance to salt ions contamination. This is because previous studies have demonstrated that NPs or nanosized materials are more effective at lower concentrations than bigger particle-based products [6, 42]. Materials with a lower NP concentration have a higher surface area-to-volume ratio than materials consisting of bigger particles, which increases material properties and functions [13]. Additionally, at lower concentrations, NPs are readily distributed evenly in the drilling mud, where they interact efficiently with other mud additives [6, 13].

2.4 Mud Weight, pH, Shear Stress, and Viscosity Measurement Procedures

The pH was assessed using a conventional pH metre, and the mud weight was obtained using a standard Fann mud balance, both of which were calibrated before measurements. These tests were each conducted twice for each of the six drilling mud samples at a given temperature, and their averages were recorded. Rheological measurements were performed using a six-speed Fann rotating 35 SA viscometer. The viscometer was re-calibrated on July 18, 2022, and measurements were taken from October to December of 2022. The stainless steel sample cup, rotor bob, torsion spring, and rotor sleeve of the viscometer may have an impact on the precision of the rheological data readings. In each case, the expected accuracy is about 0.1%. The viscometer was calibrated using a value of 1.002 mPa s for water viscosity at 1 atm and 25 °C. The dial readings (θ) and rpm data were used to predict the shear rate ($\dot{\gamma}$), shear stress (τ), and apparent viscosity (AV) using

Eqs. 1–3. The Fann 35 SA viscometer was used to read the rotor dials of the six sets of mud samples at six different rotational speeds (N): 600, 300, 100, 30, 6, and 3 rpm. Five temperature conditions were used to determine the effect of temperature on the mud samples under salt cation attack, and they include 25 °C (without oven ageing) and 120, 150, 180, and 210 °C after oven cell ageing for 16 h. For each temperature and mud sample, the Fann 35 SA viscometer measurements on a given rotation speed were carried out twice for consistency, and the corresponding average dial values were reported.

$$\dot{\gamma} = 1.7032N \quad (1)$$

$$\tau = 0.511\theta \quad (2)$$

$$AV = \frac{300\theta}{N} \quad (3)$$

where τ (Pa) = shearing stress, θ (°) = dial reading values, $\dot{\gamma}$ (s⁻¹) = shearing rate, N (rpm) = speed of rotation, and AV (mPa s) = viscosity.

2.4.1 Uncertainty and Error Estimation

Ignoring uncertainties in rheological property tests may result in minor but significant inaccuracies in estimating drilling fluid parameters. When exact rheological values are needed, the bounds of uncertainty, including an estimate of systematic error, should not be greater than 0.25% [43]. In shallow wells, the errors caused by disregarding differences in rheological parameters are minor. Mud engineers may focus on developing drilling fluid rheology for maximal rates of penetration and good hole cleaning in these wells [44]. But in HPHT, extended reach, and deepwater wells, the quality of the mud does change based on the pressure and temperature downhole. This makes both surface observations and predictions of rheological parameters less accurate. These variations may be substantial because of the narrow safety margins permitted in these wells [44]. Predicting this impact is often crucial to the successful drilling of HPHT, extended reach, and deepwater wells.

Six sets of drilling fluids were employed in the rheological measurements, and six sets of average rheological data were taken for a given mud sample at a given temperature. The fluid samples were measured using the same viscometer. After each of the six rheological tests with the six sets of drilling fluids, the samples were withdrawn from the viscometer, and the bob and cup were properly cleaned. The same six speeds of rotations with their corresponding average dial readings for each mud sample were used. In all, an average of 30 data points were obtained for a given mud sample at five temperature conditions. An average total of 180

data points were obtained for the six mud sample measurements at five different temperatures. Equations 4–7 calculate the average dial readings (θ_{ai}), standard error of the mean (SE_i), and standard deviation (SD_i) for a given dial reading, mud sample, and temperature. i denotes the varied dial readings measured between 600 and 3 rpm, and j represents which set of experiments is from 1 to 6.

$$\theta_{ai} = \sum_{j=1}^6 \theta_{ij} \tag{4}$$

$$SD_i = \frac{\sqrt{\sum_{j=1}^6 (\theta_{ij} - \theta_{ai})^2}}{5} \tag{5}$$

$$SE_i = \frac{SD_i}{\sqrt{6}} \tag{6}$$

To assess the uncertainties, each data point is normalized in relation to the average dial reading and standard deviation for a particular shear rate.

$$\theta_{nij} = \frac{\theta_{ij} - \theta_{ai}}{SD_i} \tag{7}$$

The probability density function in Fig. 3 shows that the normalized data, θ_{nij} , behaves in accordance with a normal distribution. The red curve represents a typical normal distribution, while the blue curve is the normalized average experimental data at a given temperature and all mud samples. According to Fig. 3a–e, the normalized average experimental data follows a conventional normal distribution with a belt-like shape, is symmetrical around the mean, and has the majority of values close to the centre peak. This result shows that the average experimental data are extremely close to the mean and within the area under the normal distribution curve. This inferred that the experimental data were precisely measured and that the resulting uncertainty was within the permissible range for the calibrated viscometer’s equipment.

For further analysis, Fig. 4 shows the averages of the six measured data points for each sample of mud at a given temperature, as well as the standard deviation and standard error of the mean, which were calculated from Eqs. 5 and 6. With increasing average viscometer dial readings, the standard deviation (Fig. 4a) and standard error (Fig. 4b) decrease, with a greater deviation at lower dial readings (Fig. 4a). Due to the substantial influence of diameter on torque, there is increased uncertainty in observed viscometer dial readings for lower dial values. At low dial readings, these results reveal the normal increase in experimental scatter or error when approaching the small torque region [43]. Figure 4b also shows that the standard error of the mean decreases as the standard deviation decreases. For all mud samples and temperatures, the standard deviations and standard errors are

less than 2.7% and 1.1%, respectively. In general, Figs. 3 and 4 confirm that the data cluster around the mean, very minimal experimental errors were obtained, and the rheological experiments are correct.

2.5 Measurement of Filtration Features Under API and HPHT Settings

By applying 100 psi (6.89 atm = 0.68 MPa) pressure at room temperature to an API filter press (Fann Instruments, Series 300, USA), the API fluid loss (API FL) of the prepared mud samples was measured. Each mud sample was subjected to a filtration test under HPHT settings (HPHT FL) using an HPHT filter press (Fann Instruments, Model HT4700, USA). The mud samples were heated in the mud cell using a thermostat-controlled heating jacket at predetermined temperatures of 120, 150, 180, and 210 °C and a pressure of 500 psi (3.48 MPa). The API as well as the HPHT FL were both recorded for 30 min. A vernier calliper was used to measure the filter paper’s cake thickness (API and HPHT FCT) after disassembly and cleaning.

The static filtration relationship, represented by Eq. 8, illustrates the factors influencing fluid loss, where the rate of filtration (q_r) is characterized by $\frac{dV_f}{dt}$ in mL/s. Every cake sample obtained had its q_r determined using a technique developed in a previous study [9, 21, 22]. The leftover drilling muds were quickly drained from the API apparatus after the fluid loss measurement under API setting, and deionized water of 100 mL with the filter cake already in place was fed into the chamber. The amount of water infiltrating the filter cake was recorded at orderly time interval of 3 min while the pressure was held constant at 0.689 MPa = 100 psi. The rate at which water passed via the filter medium was proportional to its filtration time, and the straight line slope is proportional to q_r . The cake’s permeability (K_c) was computed with Darcy’s equation (Eq. 9). The API filtration test used a pressure difference (Δp) of 100 psi (0.689 MPa = 6.8 atm). The filter medium area (A) of the cross section used was 0.00453 m², and the filtrate viscosity is indicated as μ_f measured at 25 °C and at 1 mPa s, which equals 1 cP. The thickness of the filter medium is known by t . An average of 72 filtration property measurements were conducted to evaluate the filtration characteristics, with each measurable parameter tested twice at a given temperature for each drilling fluid sample. Six fluid loss average measurements at five temperatures for six drilling fluid samples yielded 30 experiments. The filter cake thickness has 30 measurements as well. Furthermore, filtration rates and cake permeability measurements with the six drilling fluid samples yielded 12 experiments at 25 °C.

$$q_r = \frac{dV_f}{dt} = \frac{K_c A \Delta p}{\mu_f t} \tag{8}$$

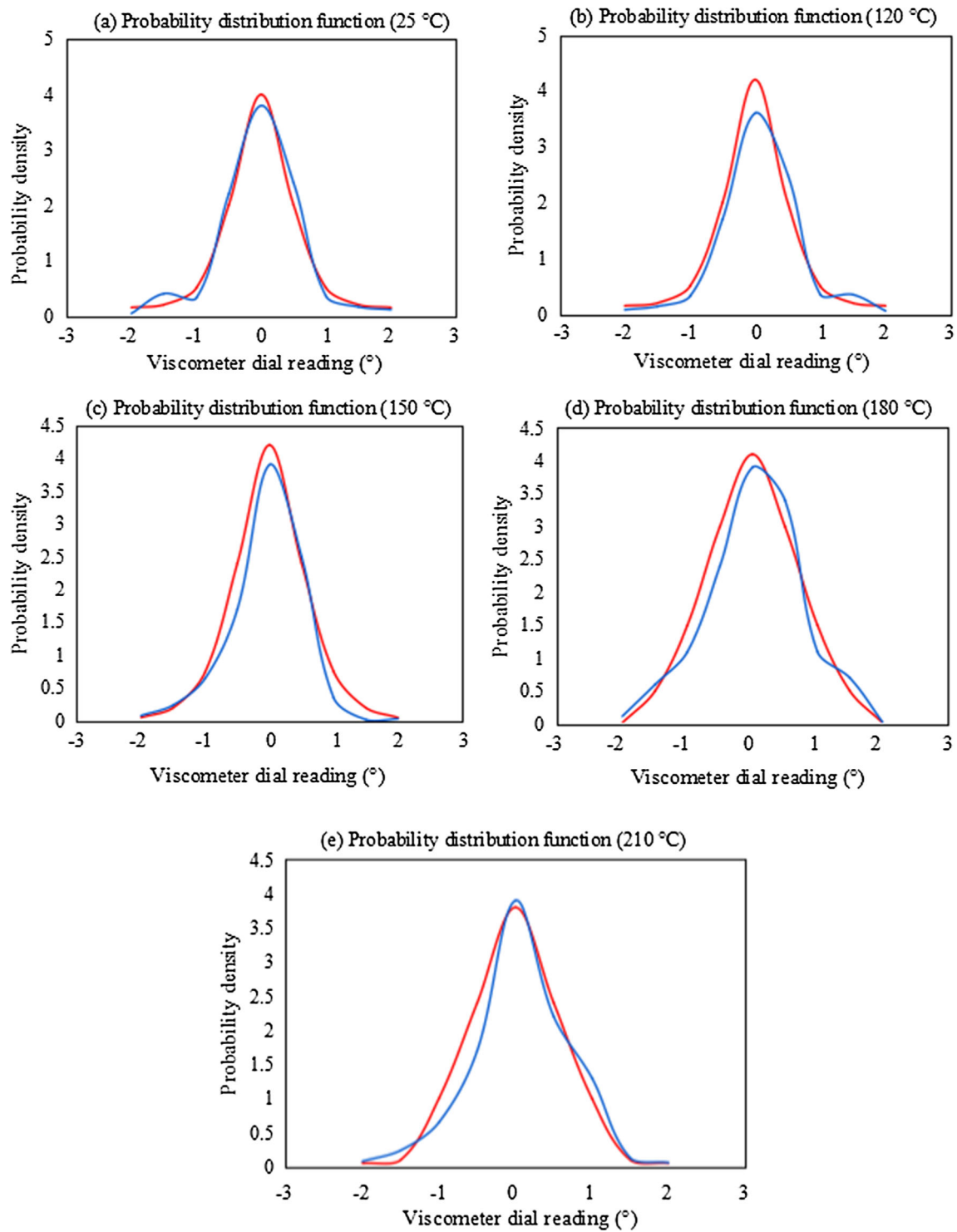


Fig. 3 Probability density function of average experimental data (blue curve) compared to a standard normal distribution (red curve) of average data sets of drilling fluids for each temperature

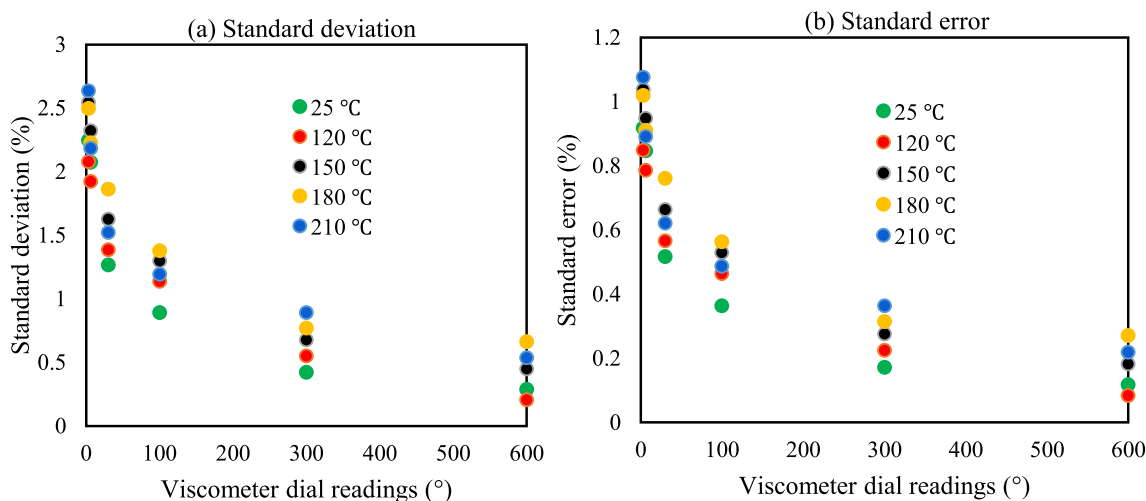


Fig. 4 a Standard deviation and b standard error as a function of average viscometer dial values for all drilling muds at five temperatures

$$K_c = \frac{q_r \mu_{ft}}{A \Delta p} \tag{9}$$

3 Research Findings and Discussions

3.1 Zeta Potential of SDS and SDS-Supported Nano-HAp Findings

The stability of NPs is one issue with nano-based drilling mud, which depends on their formulation and modification. NP surface attraction and repulsion forces are combined to determine the stability of NPs in various mud systems. The suspension becomes stable and there is no NP agglomeration when the repulsive force increases over the attractive force [30, 45]. A stable nanosuspension of the zeta potential with an absolute value of 30 mV can be created by manipulating the zeta potential [36]. The stability and suspension of NPs in drilling fluid thus increase with an increase in zeta potential independent of its absolute magnitude, owing to an increase in electrostatic repulsion force between the particles.

To assess the stability of the Nano-HAp before it was utilized in a drilling fluid system, zeta potential analysis was performed on an SDS-supported Nano-HAp sample and pure SDS powder. The purpose of the SDS zeta potential measurement is to validate the presence of SDS on the SDS-supported Nano-HAp powder. Figure 5 depicts the results of these measurements. Through the Nano-HAp functional groups, its surface was effectively coated with SDS molecules. Nano-HAp particles are electrically neutral, but in aqueous solutions, H^+ and OH^- ions along with their charged ions, are their potential determining stability parameters. The positively charged Ca^{2+} ions clumped together near the negatively charged surface of SDS, and the negatively charged

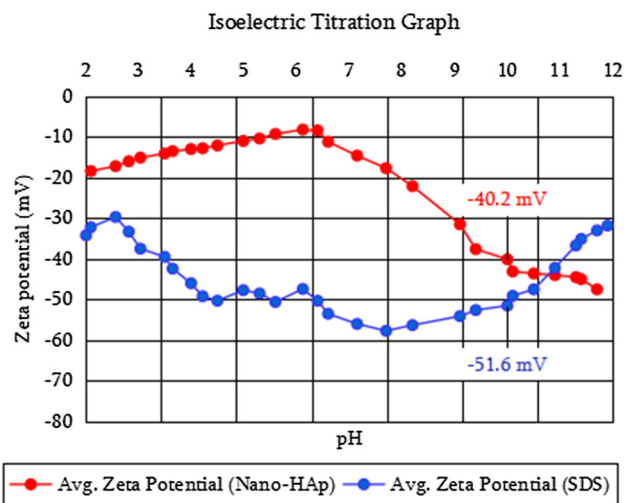


Fig. 5 Zeta potentials of pure SDS and SDS-supported Nano-HAp powder at varied pH

phosphate ions (PO_4^{3-}) stuck to SDS with the help of electrostatic forces [33]. This helped coat Nano-HAp in a stable SDS solution. As a result, SDS endows the Nano-HAp with a negatively charged surface [33]. Figure 5 demonstrates that SDS has a zeta potential magnitude that ranges from -29.8 to -57.8 mV. SDS exhibited an absolute zeta potential value of 51.6 mV at a pH of 10, which was employed to produce the Nano-HAp, indicating sufficient SO_4^- ions on the SDS surface for Nano-HAp modification [34]. When Nano-HAp particles are formed during the in situ wet synthesis technique, the high stability indicated by this zeta potential value causes increased Nano-HAp particle stability and dispersion, prevents agglomerations, and reduces the size of the Nano-HAp particles [36].

As shown in Fig. 5, the zeta potential of Nano-HAp varies from -18.5 to -47.6 mV, and it has the highest

magnitude of -47.6 mV at a pH of 11.7. The pH of the synthesis mixture was maintained at 10 using NaOH, and the SDS sulphate phase interacted with the free OH^- ions in Nano-HAp to impart a substantial negative charge on the formed particles [33]. Thus, at this pH of 10, Nano-HAp showed a high zeta potential value of -40.2 mV, suggesting strong particle stability and highlighting the modifying effect of SDS molecules in the produced apatite. After pH 7, increasing the pH of the solution increases its stability towards the less negative region. This is because hydronium ions (H_3O^+) electrostatically adsorb on Nano-HAp particles, repelling SDS particles [37]. The SDS-surface coating of Nano-HAp not only confers a high zeta potential magnitude, but it can also improve drilling mud stability in high-saline and high-temperature conditions. The Nano-HAp's surface charge load will help them remain stable in drilling mud systems for a prolonged period.

3.2 TGA Examination Findings

Typically, for every 100 m (328.1 ft.) of drilling depth, the formation temperature would rise by 2–3 °C. Currently, a reservoir with a depth of nearly 90,000 m (295,276 ft.) and a bottom hole temperature of 180–260 °C has been found [25]. As a result, one of the biggest challenges in deep and ultra-deep wells has been the tolerance of drilling fluids at very high temperatures. TGA-DTG tests of the SDS-supported Nano-HAp were done in a nitrogenous environment with three phases of thermal weight loss between 20 and 1000 °C, as shown in Fig. 6, to show how well the SDS-containing Nano-HAp particles can handle high temperatures. At temperatures between 20 and 200 °C, the first phase of breakdown of SDS-supported Nano-HAp caused a 7% weight loss due to the evaporation of lattice and adsorbed water [30, 31]. Moreover, the Nano-HAp showed a weight decline of 13% over a short TGA curve from 200 to 320 °C. At this point, the SDS molecules and OH^- ions were thermally decomposed [33]. According to previous findings, the SO_4^- and alkyl groups of SDS molecules can survive up to 200–320 °C before they are entirely destroyed [33]. These findings are consistent with the TGA behaviour of pure SDS particles reported in previous studies [33, 34].

At 750 °C, Nano-HAp undergoes a final point of breakdown in which all its molecular chains and ions (PO_4^{3-} and CO_3^{2-}) are fully destroyed [31], and it gradually decomposes by 7% from 320 °C up to 750 °C. Overall, the SDS-supported Nano-HAp shows an overall weight loss of 20% from 20 to 320 °C and 27% from 20 to 750 °C. The derivative weight curve (DTG) showed that three peaks correspond to the three decomposition steps of the SDS-supported Nano-HAp. The DTG peak at 70 °C is due to the released adsorbed water molecules. The peak at 270 °C corresponds to the complete decomposition of OH^- ions and SDS alkyl and sulphate

chains. The final decomposition peak at 850 °C is caused by the total degradation of PO_4^{3-} and CO_3^{2-} moiety in the particles of SDS-supported Nano-HAp layer. These findings support previous research [31, 46–48] and confirm that the SDS molecules are contained within the Nano-HAp structure [29, 33]. Thus, the TGA/DTG data corroborate the Nano-HAp's strong and high thermal stability, suggesting it can uphold excellent thermal stability for a prolonged period during drilling operations in deepwater and high-temperature wells.

3.3 PSD Results of Particles of SDS-Assisted Nano-HAp

The results of the PSD of SDS-aided Nano-HAp powder are shown in Fig. 7. Particle size analysis on the formed HAp product with anionic surfactant showed a unimodal distribution, with an average size of 110.4 nm and a standard deviation (σ) of 38.3 nm. The PSD analysis of most HAp powders without surfactant reveals a bimodal distribution of larger particle sizes [42]. The largest frequency volume of the particles corresponds to a peak frequency of 105.7 nm. Anionic SDS modifies the surface geometry of the Nano-HAp and suppresses its nanocrystal growth. SDS bilayers are formed on the surface of Nano-HAp to shield its surface from crystal growth [29, 33]. With a high zeta potential of -40.2 mV achieved at a pH of 10 (see Fig. 5), the shielding promotes the formation of smaller Nano-HAp particles, which are mostly spread from 700 to 600 nm in diameter. These results are in agreement with PSD data of commercial HAp and HAp synthesized with surfactants in previous research [29, 33, 34, 37]. The data of PSD of the particles of Nano-HAp in this study is desirable for drilling operations, particularly for fluid loss control [6].

3.4 FTIR Spectra of Nano-HAp Particles

To highlight the modifying presence of SDS in the produced particles of Nano-HAp, the bond connections and moiety of both particles of Nano-HAp and SDS were identified using FTIR investigation (Fig. 8). The transmittance infrared spectra in the 4000–400 cm^{-1} bands show that the produced Nano-HAp particles had more than one functional group and SDS components. The peak assignments related to the examined pure SDS product and the synthesized powder of Nano-HAp containing SDS are illustrated and described in Table 2. According to Table 2 and Fig. 8, the existence of the phosphate phase (PO_4^{3-}) in the HAp was proven by the band that occurred at 1101.25 cm^{-1} , and this bond of P–O related to the PO_4^{3-} moiety asymmetrically stretched, allowing this transmission to occur [31]. The presence of carbonate was revealed by the peak that occurred at 1402.24 cm^{-1} , and this peak is connected to the stretching C–O asymmetric of

Fig. 6 TGA/DTG curves of pure SDS and particles of SDS-supported Nano-HAp

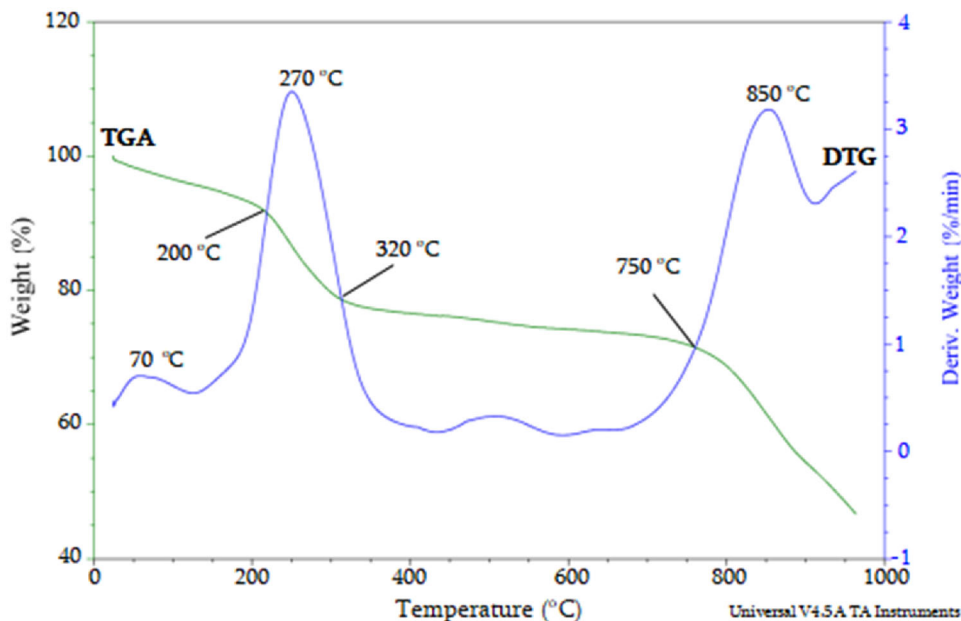
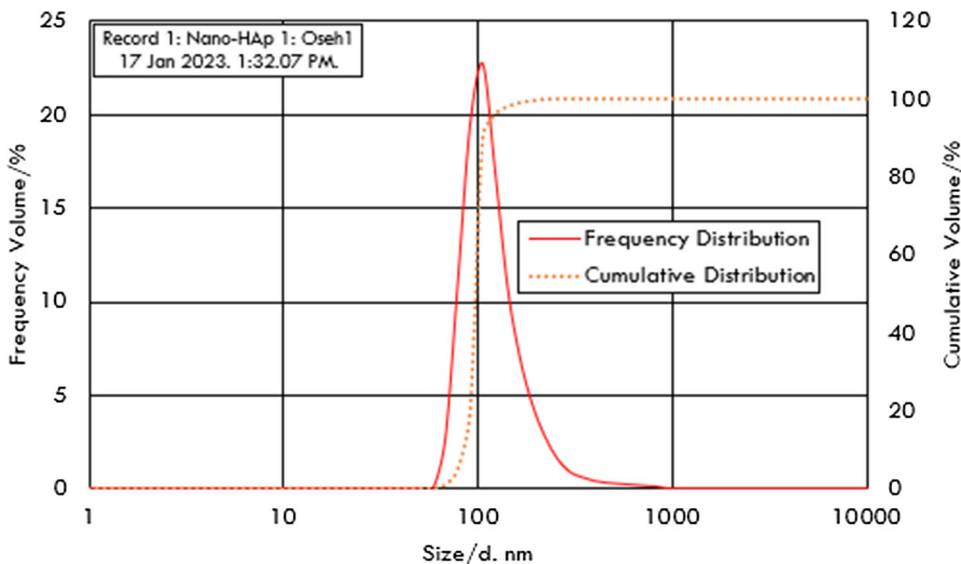


Fig. 7 PSD curves of SDS-assisted Nano-HAp powder



the CO_3^{2-} moiety [47]. Two closely related peaks (1246.06 and 1213.23 cm^{-1}) were induced by skeletal vibration of the bridge S–O and –S=O symmetric stretching of SO_4^- groups of SDS, respectively [42]. Between 650 and 700 cm^{-1} , the Nano-HAp particles did not exhibit any transmission peaks of C–O, suggesting that no calcite was formed [48]. According to Fig. 8, the peak assignments (in blue) indicate the bands that belonged to Nano-HAp without surfactant, while those (in black) belonged to SDS molecules that are in the synthesized Nano-HAp, thus highlighting the modified existence of molecules of SDS in the particles of the Nano-HAp product.

3.5 XRD Findings

The elements and peak form of SDS-aided Nano-HAp nanopowder was examined with an XRD analysis, and the outcomes are shown in Fig. 9. The diffraction peaks obtained in laboratory are consistent with HAp crystals with a hexagonal structure [29, 31]. The diffraction patterns are typically HAp, in accordance with reference HAp (ICDD@ 9-0432) and literature data, and they match surfactant-aided HAp results of previous research produced in situ using the chemical precipitation method [29, 31, 32, 37, 42]. The XRD patterns presented did not reveal the transformation of HAp into secondary phases such as tricalcium phosphate or

Fig. 8 FTIR spectra of synthesized SDS-assisted Nano-HAp particles and SDS powder

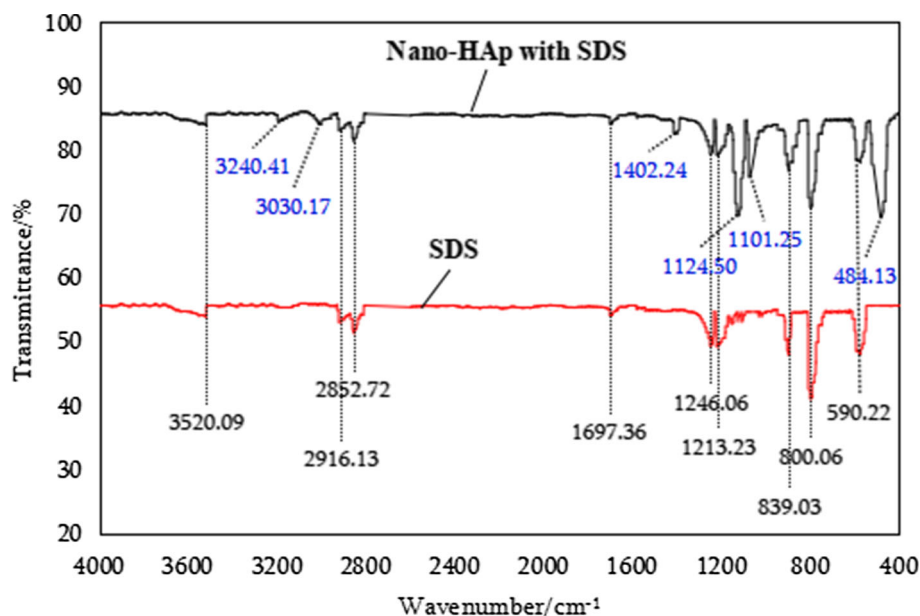


Table 2 Important functional groups assignment of formed Nano-HAp particles

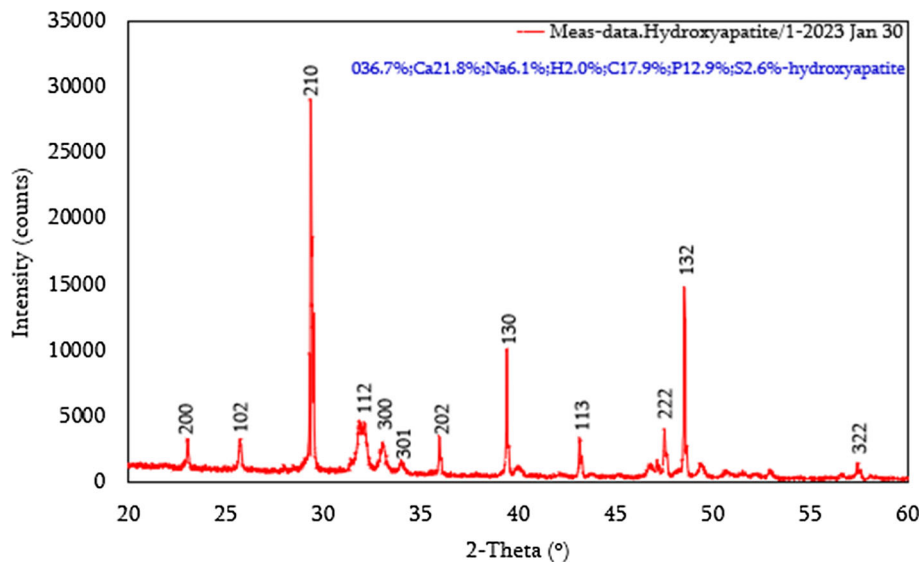
Transmission peak/cm ⁻¹	Vibration mode	Functional groups	References
3520.09	Ion stretching	H–OH	[48]
3240.41	Ion stretching	– OH	[48]
3030.17	H ₂ O molecules ions	– OH	[48]
2916.13	C–H stretching and bending mode	– CH ₂	[33]
2852.72	C–H stretching and bending mode	– CH ₃	[33]
1697.36	CH ₂ stretching and bending mode	– CH ₂	[33]
1402.24	C–O asymmetric stretching	CO ₃ ²⁻	[47]
1246.06	S–O anti-symmetric stretching	SO ₄ ⁻	[34]
1213.23	– S=O symmetric stretching	SO ₄ ⁻	[34]
1124.50	C–O symmetric stretching	CO ₃ ²⁻	[38]
1101.25	Asymmetric stretching of P–O bond	PO ₄ ³⁻	[31]
839.03	C–O symmetric stretching and C–H bending	– CH ₂ , CO ₃ ²⁻	[42]
800.06	S–O bending mode	SO ₄ ⁻	[33]
590.22	Symmetric stretching of P–O bond and C–H bend	– CH ₂ , PO ₄ ³⁻	[29]
484.13	Asymmetric –O–P–O bending vibration	PO ₄ ³⁻	[31]

calcite after drying at 60 °C, indicating good product formation [31]. The peak patterns of [130], [210], and [132] shown by the XRD spectrum are quite sharp, proving the formed Nano-HAp crystals to be well-developed with a high degree of purity and crystallinity [31]. These peak patterns of diffraction are an excellent example of how a hexagonal arrangement with primitive spacing of lattices occurs [42], and SDS particles intercalated to produce bilayered surfactant Nano-HAp [33]. Accordingly, typical Nano-HAp particles with hexagonal structures were produced, and they

stayed stable, as indicated by zeta potential findings (refer to Fig. 5).

The organic compound SDS has a molecular formula of CH₃(CH₂)₁₁OSO₃Na, while pure HAp formula is Ca₁₀(PO₄)₆(OH)₂ [31, 33]. In Fig. 9, the elemental compositions in percentages represented in blue demonstrate that the particles of SDS-assisted Nano-HAp are composed of the constituents of SDS, calcium, and phosphorus, and they have a good stoichiometry ratio similar to the stoichiometric ratio of pure hydroxyapatite of 1.67. The components

Fig. 9 Synthesized particles of Nano-HAp powder identified by XRD technique



of SDS in the formed product are carbon (C), sulphur (S), and sodium (Na), which are absent in the pure HAp molecular formula, demonstrating that the formed product contains SDS elements.

3.6 HR-TEM Examination of Nano-HAp Particles

The structural morphology of synthesized particles of SDS-supported Nano-HAp was observed by HR-TEM (Fig. 10). According to Fig. 10a, the synthesis procedure resulted in the formation of Nano-HAp crystals in a small rod-like shape, and the length of the rods is between 20 and 160 nm, while their diameters are from 10 to 30 nm, according to Fig. 10b. Using the J-icon suite, the rods' diameters and lengths were measured, and origin-package was used to examine their distribution (Fig. 10b). Based on these measurements, the SDS-assisted Nano-HAp formed has an 80.0 nm and 18 nm average length and diameter of the rods, respectively. This gives a 4.5 nm value for an aspect ratio defined by the ratio of the rod length average to that of the diameter [33]. These results agree with those of earlier studies that have been conducted [33, 34, 42]. The morphology of the particles of Nano-HAp in short-rod form is similar to the morphology of stoichiometric HAp with surfactants in earlier studies, since most HAp powders generated without surfactants display an agglomeration tendency [31, 34].

The unique structure of Nano-HAp could be attributed to the anionic SDS, which promotes the development of an ordered nanostructure in the aqueous medium to serve as a control template for the produced Nano-HAp particles [33, 34]. The rod-length shape and size of the formed Nano-HAp particles lie within the nanoscale domain, which is often

employed in the drilling of oil and gas wells [42]. This is due to the fact that the formation pore diameters are in the range of micrometres. This suggests that the fabricated particles of SDS Nano-HAp might be suitable for drilling applications, particularly in terms of decreasing filtrate loss [42]. In addition to this, an EDX analysis was carried out to gain a better understanding of the components that constitute the Nano-HAp particles.

3.7 Elemental Composition of Synthesized Particles of Nano-HAp Identified by EDX

The EDX examination was conducted to ascertain the modifying existence of the molecules of SDS in the synthesized powder of Nano-HAp through understanding the elemental composition of the SDS-assisted Nano-HAp (Fig. 11). The investigation shows both the elemental composition of SDS and calcium-phosphate ceramic in the morphology of the Nano-HAp powder. The elements shown are O (oxygen), Ca (calcium), P (phosphorus), S (sulphur), C (carbon), and Na (sodium), all of which are assigned to the produced SDS-supported Nano-HAp. Whereas Ca, O, and P are pure HAp elements, Na, S, C, and O are components of anionic SDS, demonstrating the existence of SDS in the formed HAp product. The Ca/P ratio (inset table) in Fig. 11 showed a Ca/P ratio of around 1.69, which is a few fractions away from pure HAp's 1.67, implying that the SDS surfactants may have influenced the Ca/P ratio [33, 34]. This observed elemental composition and Ca/P ratio is consistent with those obtained in the XRD patterns (see Fig. 9).

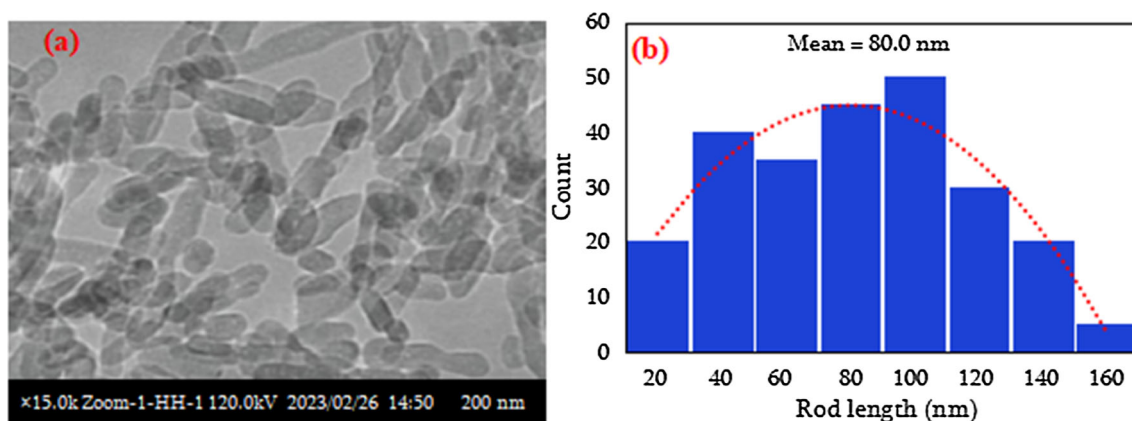
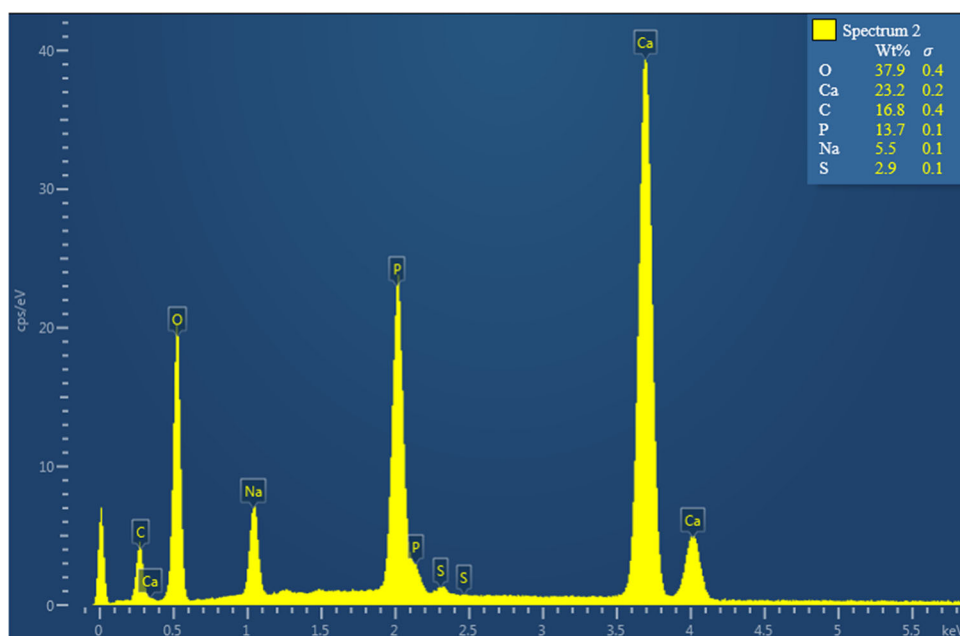


Fig. 10 a HR-TEM image and b rod length distribution of Nano-HAP powder

Fig. 11 Elemental composition of Nano-HAP revealed by EDX



4 Salt cations Mechanism on BN-Based Water Solution at $\text{Ca}^{2+}/\text{Na}^+$ Conditions

4.1 Density and pH of Drilling Muds at 25 and 120 °C

CaCl_2 and NaCl salts weighing 5 wt% each were added to BN and BN/HAp muds to analyse their density and pH behaviour. The findings are shown in Table 3. The salt components had minimal effect on the BN's density property at both 25 and 120 °C (Table 3). Nano-HAp at 25 °C only slightly increased the density by 1.16%, whereas NaCl and CaCl_2 showed a higher decrease of 4.66% and 2.33%, respectively. At 120 °C, the density trend of the mud samples increased above that of BN, except for the BN/Na sample, which decreased. The presence of Nano-HAp in BN demonstrated that the salt contaminants were screened. For instance, Nano-HAp raised the density of the BN by 7.42%, and the BN/Na and BN/Ca

samples had greater densities with the HAp than with the BN alone at both temperatures.

The variation of pH with BN-WBMs under salt contamination and Nano-HAp impact is shown in Table 3. In general, as the synthesized particles of Nano-HAp and inorganic salts were introduced into the water-BN-based solution, the pH decreased slightly at both temperatures, with CaCl_2 having the most impact. The pH was reduced from 9.61 to 8.93 when a Nano-HAp concentration of 0.5 wt% was used, with a change of 7.1% at 25 °C. The existence of Ca^{2+} and Na^+ in the mud system belonging to BN/HAp caused the pH to drop almost twice at both temperatures. When NaCl and CaCl_2 were added to the BN, the pH dropped by 8% and 20%, respectively. The pH of the BN was decreased when Ca^{2+} and Na^+ were introduced as a result of the breakdown of pre-existing CaCl_2 and NaCl precipitates, which prevents the formation of new chloride salts [18, 21]. When Ca^{2+} and

Table 3 Average pH and density data of BN and BN/HAp with salt contaminants

Mud sample	pH	Density (ppg)							
		25 °C		120 °C		25 °C		120 °C	
		% Δ pH	% Δ pH	% Δ Density					
BN	9.61	–	9.61	–	1.031	–	0.971	–	–
BN/Na	8.88	– 7.60	8.85	– 7.91	0.983	– 4.66	0.959	– 1.24	–
BN/Ca	7.69	– 19.9	7.68	– 20.1	1.007	– 2.33	0.985	+ 1.44	–
BN/HAp	8.93	– 7.08	8.93	– 7.08	1.043	+ 1.16	1.043	+ 7.42	–
BN/HAp/Na	8.23	– 14.4	8.21	– 14.6	1.019	– 1.17	1.007	+ 3.71	–
BN/HAp/Ca	8.15	– 15.2	8.14	– 15.3	1.025	– 0.58	1.019	+ 4.80	–

Na⁺ continue to precipitate, BN reacts with the salts, lowering the pH. The little drop in pH across all mud formulations at 120 °C showed that more ions were dissociated, leading to higher contents of H⁺ or H₃O⁺ [29].

4.2 Rheological Behaviour of Nano-HAp in BN-Based Suspension Under Salt Cations at 25 and 120 °C

Montmorillonite (MMT), a clay mineral with platelets ranging in size from 1 to 500 nm, makes up sodium BN. It was reported that the negative charge on the surface of BN platelets is caused by lattice cation isomorphism [5, 18]. Surface charges on the BN platelet edges are affected by pH [18, 22]. The platelet edges will be positively charged in an acidic environment and negatively charged in an alkaline medium. The amphoteric Al–OH and Si–OH groups on the BN platelet edges, which may undergo either protonation or deprotonation in either direction, are responsible for these charges [9]. When BN platelets are dried and layered in a sandwich fashion with sodium ions (Na⁺) between each layer, sodium BN microparticles are created [18]. Edge-edge, edge-face, and face-face are the three modes of association that BN platelets may have in a well-dispersed aqueous solution, which are all influenced by electrostatic attraction and repulsion forces, hydrogen bonds, and the van der Waals force [22]. The three common shapes that BN platelets may take are aggregated, flocculated, and exfoliated [18–22]. These shapes have an impact on the physical properties, rheology, tribology, and filtration features of fluids. Many factors, such as pH, age, salinity, temperature, and BN concentration, have a significant impact on the drilling fluid formed filter cake medium, fluid loss, and rheology [18, 22].

Figure 12 shows the manner in which NaCl and CaCl₂ affect the viscosity and shear stress of BN drilling muds, while Table 4 displays the percentage variations in viscosity between BN-based water suspension after salt addition. The BN suspension has a viscosity of 5.5 and 4.3 mPa s at 25 and 120 °C, respectively, when 4.8 wt% of BN is added to 350 mL of deionized water. The BN swells as a consequence of its interactions with the water molecules, which create a

diffuse double layer. The connecting layers between the solid particles thicken as the BN expands, increasing the water's viscosity [22]. The impact of the salts on the BN was examined using the BN-WBM. Regardless of the presence of Ca²⁺ and Na⁺, CaCl₂ and NaCl had an impact on the BN's shear stress (Fig. 12a, b) and viscosity (Fig. 12c, d). The findings reveal that contamination with NaCl and CaCl₂ raises the shear stress/shear rate and viscosity/shear rate curves of BN-WBMs at all shear rates. Under 1022 s⁻¹ shear rate, CaCl₂ and NaCl-contaminated BN-WBMs unduly increased the viscosity by 2725% and 1956%, respectively, under ambient conditions (Table 4). The flat-face (negatively charged) and edge-surface (positively charged) surfaces of BN platelets interact with the positive ions CaCl₂ and NaCl, resulting in edge-to-face and edge-to-edge (flocculation process). A “house-of-cards” arrangement will arise as a consequence of the flocculation process, thereby resulting in a higher viscosity of salt-contaminated BN-WBMs [25].

Temperature increase will destabilize the equilibrium of interparticle attractive and repulsive interactions, increasing the degree of dispersion and flocculation of the mud systems, keeping the particles apart, and lowering viscosity [25]. Table 4 and Fig. 12 reveal that BN-water suspensions with salt contamination and Nano-HAp had lower viscosities and shear stresses at 120 °C because BN suspension hydration shells were partially destroyed [49]. At a shear rate of 1022 s⁻¹, NaCl and CaCl₂ conditions adversely modified the BN viscosity towards an increasing trend by 21-fold (1964%) and 18-fold (1700%), respectively. These results suggest that the performance of BN-water suspension under CaCl₂ and NaCl assault would diminish throughout drilling operations. The salts' adverse impacts on BN particle dispersion, hydration, and flocculation will render the BN solution ineffective for suspending and conveying cuttings [25, 49]. In addition, partial fluid loss, loss of circulation, stress on the bit, high pump power requirements, and fracture formation may result.

When BN-water solutions were exposed to salt cations, the viscosity of the Ca²⁺-contaminated solution decreased by 42.9% from 25 to 120 °C, whereas the viscosity of the Na⁺-attacked suspension decreased by 31.5% (Table 4).



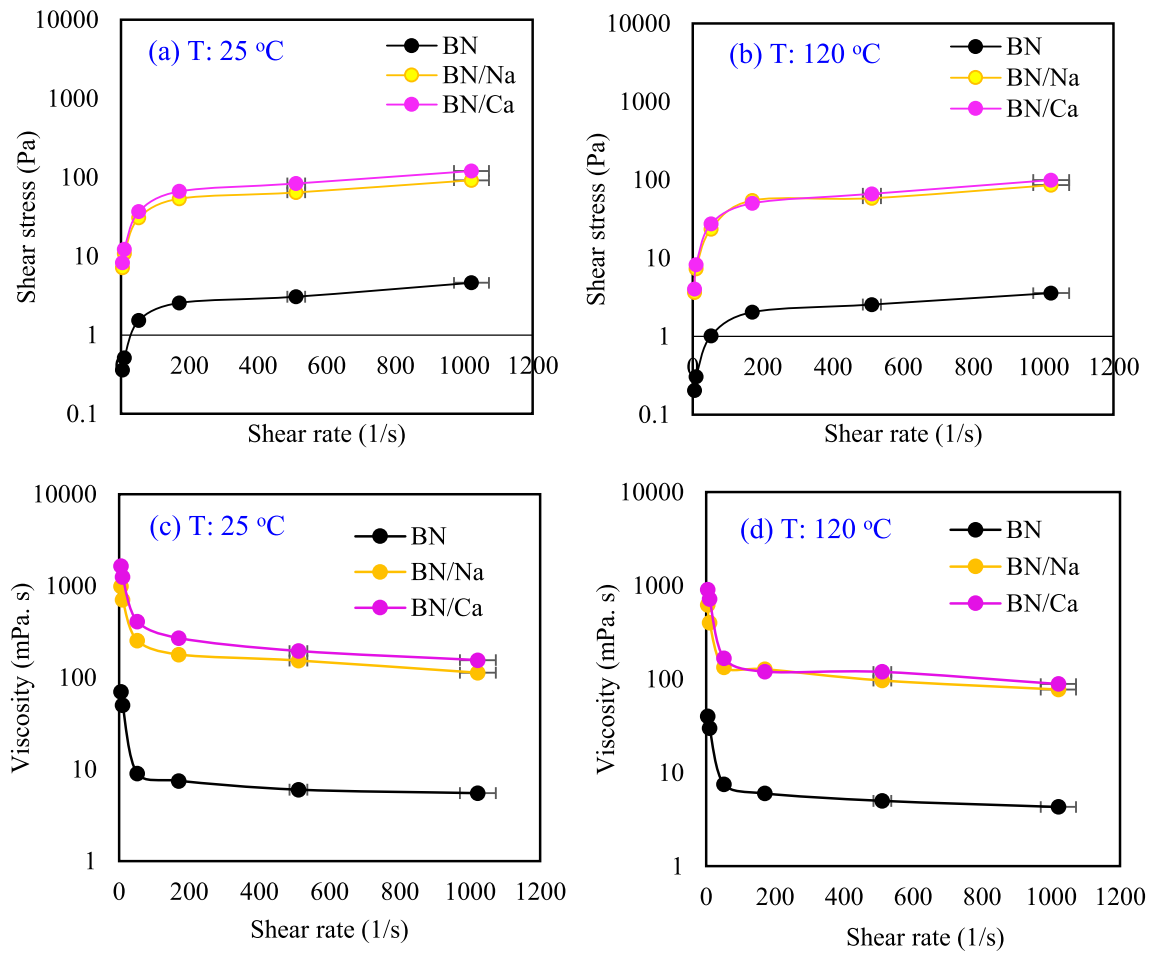


Fig. 12 BN-salt-contaminated WBMs: **a** shear stress at 25 °C; **b** shear stress at 120 °C; **c** viscosity at 25 °C; and **d** viscosity at 120 °C

Table 4 Percentage change in the values of the viscosity of BN with salt contaminants

Fluid sample	Shear rates (s ⁻¹)	AV (mPa s) before ageing		AV (mPa s) after ageing		% variation in viscosity
		25 °C		120 °C		% ΔAV
						% ΔAV (25–120 °C)
BN	5.11	70	–	40	–	– 42.9
	511	6.0	–	5.0	–	– 16.7
	1022	5.5	–	4.3	–	– 21.8
BN/Ca	5.11	1655	+ 2264	905.2	+ 2163	– 45.3
	511	195.3	+ 3155	119.7	+ 2294	– 38.7
	1022	155.4	+ 2725	88.78	+ 1965	– 42.9
BN/Na	5.11	992.4	+ 1318	621.8	+ 1455	– 37.3
	511	153.6	+ 2460	96.8	+ 1836	– 36.9
	1022	113.1	+ 1956	77.43	+ 1700	– 31.5

Monovalent Na^+ ions have a lower positive charge impact than divalent Ca^{2+} cations, making their contamination of BN-WBM have the least detrimental influence on the system viscosity. Additionally, since Ca^{2+} is more coarse than Na^+ , it is more reactive than Na^+ . Therefore, CaCl_2 contamination reduces BN-based suspension viscosity more than NaCl contamination does [18].

4.3 Filtration Properties of BN-Based Suspension Under Salt Cations at 25 and 120 °C

The filtration behaviour of the salt-contaminated BN-based drilling muds is shown in Fig. 13. The percentage variations existing in these drilling muds are summarized in Table 5, which shows that BN is sensitive to salt cations assault. After 30 min of filtration, BN-based water suspension had an API FL of 22 mL and HPHT FL of 31 mL. With the presence of NaCl , these values, respectively, under API and HPHT settings rise to 56 mL and 90 mL. Similarly, it also increased to 71 and 118.2 mL with CaCl_2 (Fig. 13a, b). CaCl_2 and NaCl , respectively, increase the volume of filtrate loss of BN by 222–281% and 155–190% between 25 and 120 °C. Compared to Na^+ , Ca^{2+} generated greater filtrate losses. BN-water solution showed an enormous fluid loss of 22 and 31 mL, respectively, during API and HPHT filtration tests at 100 and 500 psi differential pressures. At 120 °C, BN particles were hydrated, aggregated, and coalesced, which is a significant problem for mud compositions under deep and ultra-deep wells [18, 49].

Figure 13c and d show the thickness of the filter cake when the conditions are API and HPHT, respectively. Figure 13e and f show the properties of the filter cakes. Figure 13c and d show that the API and HPHT FL have thick and high-permeable filter cakes. Under NaCl and CaCl_2 conditions, the BN cake thickness rose by 180–200% and 230–260%, respectively. This is because CaCl_2 and NaCl clumped together and flocculated, respectively, creating loose filter cakes that allow high volumes of water to pass through. Figure 13e and f showed that the API FL of the BN had a filtration rate of 0.00772 mL/s and a permeability of 0.00281 mD. When 5.0 wt% of NaCl was added, these values increased by 130% and 323.5%, respectively. Under similar CaCl_2 concentration, the filtration rate and cake permeability increased by 177% and 1063%, respectively.

4.4 Salt Contamination Process of BN-Based Suspension at 25 and 120 °C

The potential salt-contaminant process of BN particles is shown in Fig. 14. It demonstrated that Na^+ and Ca^{2+} ions significantly affect the dispersion of BN particles from exfoliation to flocculation and aggregation behaviours, respectively [18–20]. According to Fig. 14a–c, electrostatic forces exerted

a significant attraction between the edge face surfaces of the negatively charged BN platelets, allowing the BN particles to partly penetrate the exfoliated morphology. The monovalent Na^+ cations (Fig. 14c) caused shear-induced BN flocculation by changing how the BN was spread out, whereas the Ca^{2+} divalent cations contributed to the aggregation of BN particles by making the BN suspension less stable and more spread out (Fig. 14a).

Furthermore, CaCl_2 acted as a cross-linking agent to produce a "face-to-face" arrangement between the platelets of two BN (Fig. 14a), resulting in the aggregation of the particles of BN [18]. The interaction between the negatively charged surfaces of the particles of BN resulted in the absorption of Na^+ when NaCl was added (Fig. 14c). The "edge-face" attachment technique resulted in a flocculated microstructure [18, 25]. The change in the morphology of the particles of BN dispersion from an exfoliated state (Fig. 14c) to an aggregated state (Fig. 14a) and flocculated state (Fig. 14c) increases the force of attraction between the particles of BN, causing the water-BN-based solution to become overly viscous. Furthermore, the flocculation and aggregation that resulted decreased the BN platelets' filtration inhibitory capacity. This resulted in significantly increased loss of drilling fluid and the formation of loose filter medium and very thick cakes in the presence of NaCl and CaCl_2 concentrations [25, 49].

4.5 Rheological Behaviour of BN/HAp Under Na^+ and Ca^{2+} Cations

Figure 15 shows Nano-HAp's salt resistance in BN-based water solution rheology. Salt-dependent mud of BN resulted in the aggregation and flocculation of BN particles under CaCl_2 and NaCl concentrations, and these conditions affect BN particle dispersion [11, 25]. Nano-HAp (with several oxygen sites, CO_3^{2-} , PO_4^{3-} , OH^- , and an SO_4^- sulphate layer) can physically attach to BN platelets and protect them from salt contamination-induced flocculation and aggregation [11]. Figure 13 displays the manner in which NaCl and CaCl_2 salts affected the shear stress and viscosity of BN/HAp's drilling muds. Under salt contamination, the 0.5 wt% concentration of Nano-HAp in 4.8 wt% of the BN-water suspensions raised the shear stress curves as the shear rate increased. It also reduces the viscosity values with an increase in the shear rate of the BN-water solutions. It increased the shear thinning of BN-water solutions at 25 and 120 °C and protected BN edge face surfaces from salt cation attack. Nano-HAp high dispersion and stability in BN-based suspension allow the physical binding of the particles to the edges and faces of BN platelets to prevent Ca^{2+} and Na^+ ion-induced BN aggregation and flocculation [18, 20–25].

Table 6 shows that owing to Nano-HAp's strong dispersion stability, at all shear rates, the BN viscosity rose by

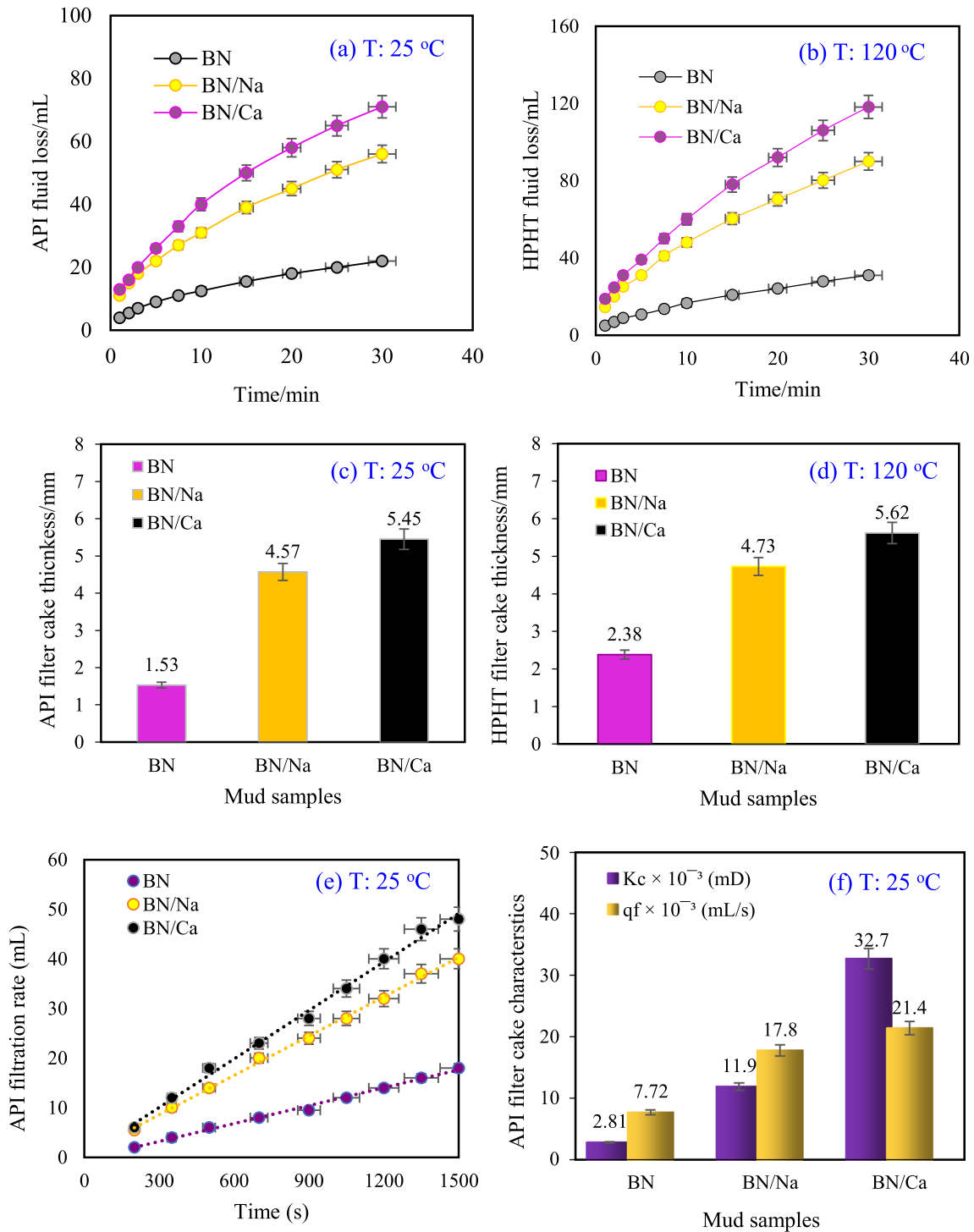


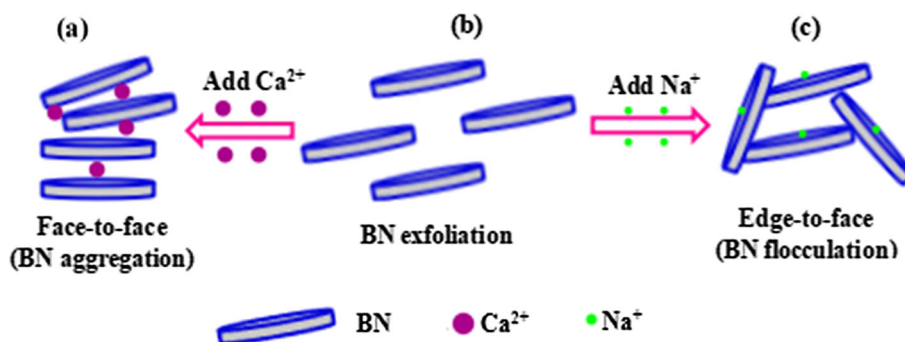
Fig. 13 BN-salt-contaminated WBMs showing the values of filtration features **a** fluid loss at 25 °C; **b** fluid loss at 120 °C; **c** cake thickness at 25 °C; **d** cake thickness at 120 °C; **e** API filtration rate; and **f** formed

API filter cake characteristics. Note: In **(e)**, the slopes of the dashed lines indicate the filtration rate of the precipitated filter cake

Table 5 Percentage change in the filtration data of BN with salt contaminants

Mud sample	Temperature	Filtrate loss (mL/30 min)	%ΔFL	Cake thickness (mm/30 min)	%ΔFCT
BN	API @ 25 °C	22	–	1.53	–
	HPHT @ 120 °C	31	–	2.38	–
BN/Na	API @ 25 °C	56	+ 154.5	4.57	+ 198.6
	HPHT @ 120 °C	90	+ 190.3	4.73	+ 183.2
BN/Ca	API @ 25 °C	71	+ 222.7	5.45	+ 256.2
	HPHT @ 120 °C	118.2	+ 281.3	5.62	+ 236.5

Fig. 14 Mechanism of BN-salt contamination process (saline environment): **a** CaCl₂, **b** exfoliated microstructure, and **c** NaCl. BN platelets are shown by the blue/ash plate



45–186% (25 °C) and 107–186% (120 °C). By introducing Nano-HAp at a concentration of 0.5 wt%, the rheological behaviour of BN-based suspensions that are reliant on salt is reduced (Fig. 15). Under salt conditions, the viscosity of BN/HAp is considerably reduced in comparison with BN mud (Table 6). The viscosities of the BN/HAp, BN/HAp/Na, and BN/HAp/Ca-based water solutions were 10, 40, and 50 mPa s, respectively, under ambient conditions after the completion of testing at a shear rate of 1022 s⁻¹. While CaCl₂ and NaCl concentrations increase the viscosity of BN by 28 and 20 times, respectively, at 1022 s⁻¹ (see Table 5), the impact of these concentrations is < tenfold in BN-based solutions containing 0.5 wt% Nano-HAp (Table 6). Similarly, at 120 °C, the viscosity of the salt-contaminated BN/HAp mud systems is less than ninefold (Table 6), as opposed to the salt-contaminated BN-WBMs, where Na⁺ and Ca²⁺ cations, respectively, induce a rise in viscosity of > 17-fold and 20-fold (see Table 5).

The flat-face surface, which is typically negatively charged, and the edge surface, which may be positively charged, are the two distinct surfaces that plate-shape particles like BN are said to have [18]. Three alternative associations between these particles are possible: face-to-face, edge-to-edge, and edge-to-face. Particles may be linked in these several ways concurrently, or one kind may prevail [22, 25]. The edge-face contact between the Nano-HAp particles and BN platelets will occur when ions like SO₄⁻ and OH⁻ are present in BN-WBMs. This will cause a dispersed and stabilized system to develop, which will increase the viscous properties of the muds [18, 49]. Additionally, in the

presence of SO₄⁻ and OH⁻ ions, Ca²⁺ and Na⁺ can interact with free water molecules and BN platelets to form hydrate envelopes around ions. These envelopes reduce the interaction between free water molecules, compress the double layer of BN particles, and prevent BN platelets from linking together [25]. As a result, the salt-contaminated BN-WBMs became less viscous when Nano-HAp particles were present.

The CaCl₂-contaminated BN suspension is the most negatively impacted by 120 °C, as seen in Fig. 15. The partial breakdown of the BN hydration shell and reduced hydration of NaCl and CaCl₂ at 120 °C counterions reduce the viscosity [24, 25]. Increased aggregation of BN platelets and a compressed electric double layer between BN particles will reduce solid volume and allow BN aggregates to move freely through the aqueous phase, lowering friction between the particles [2, 25]. These activities will reduce drilling mud viscosity after 16 h of prolonged exposure at 120 °C. In summary, the 0.5 wt% Nano-HAp used served as an anti-salt agent, and the viscosity declined by just 11% from 10 to 8.9 mPa s throughout a temperature range of 25–120 °C, indicating its potential for HPHT drilling. Similarly, adding Nano-HAp at a concentration of 0.5 wt% to salt-contaminated BN suspensions decreased the viscosity by 25 and 26% under NaCl and CaCl₂ conditions, which might be relevant to drilling deep and ultra-deep formations [22, 24].

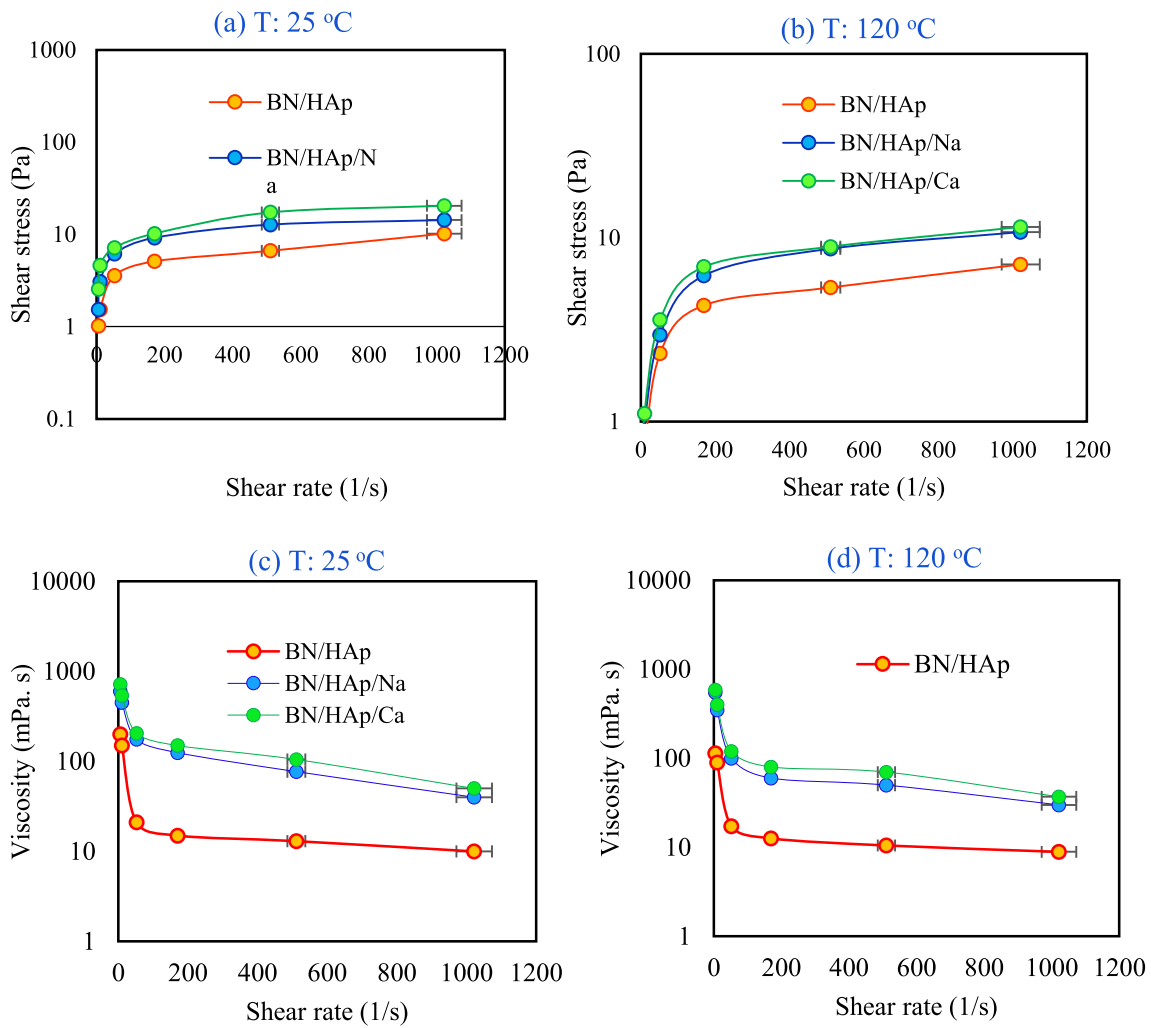


Fig. 15 BN/HAp-salt-contaminated WBMs: **a** shear stress at 25 °C; **b** shear stress at 120 °C; **c** viscosity at 25 °C; and **d** viscosity at 120 °C

Table 6 Percentage change in the values of the viscosity of BN/HAp with salt contaminants

Fluid reference	Shearing rates (s ⁻¹)	AV before ageing (mPa s)	% variation in viscosity	AV after ageing (mPa s)	% variation in viscosity	% variation in viscosity
		25 °C	% ΔAV	120 °C	% ΔAV	% ΔAV (25–120 °C)
BN/HAp	5.11	200	+ 186	114.3	+ 186	- 42.9
	511	13	+ 117	10.5	+ 110	- 19.2
	1022	10	+ 45	8.9	+ 107	- 11.0
BN/HAp/Ca	5.11	720	+ 929	589	+ 1373	- 18.2
	511	105	+ 1650	70	+ 1300	- 33.3
	1022	50	+ 809	37	+ 761	- 26.0
BN/HAp/Na	5.11	600	+ 757	550	+ 1275	- 8.33
	511	77	+ 1183	50	+ 900	- 35.1
	1022	40	+ 627	30	+ 598	- 25.0

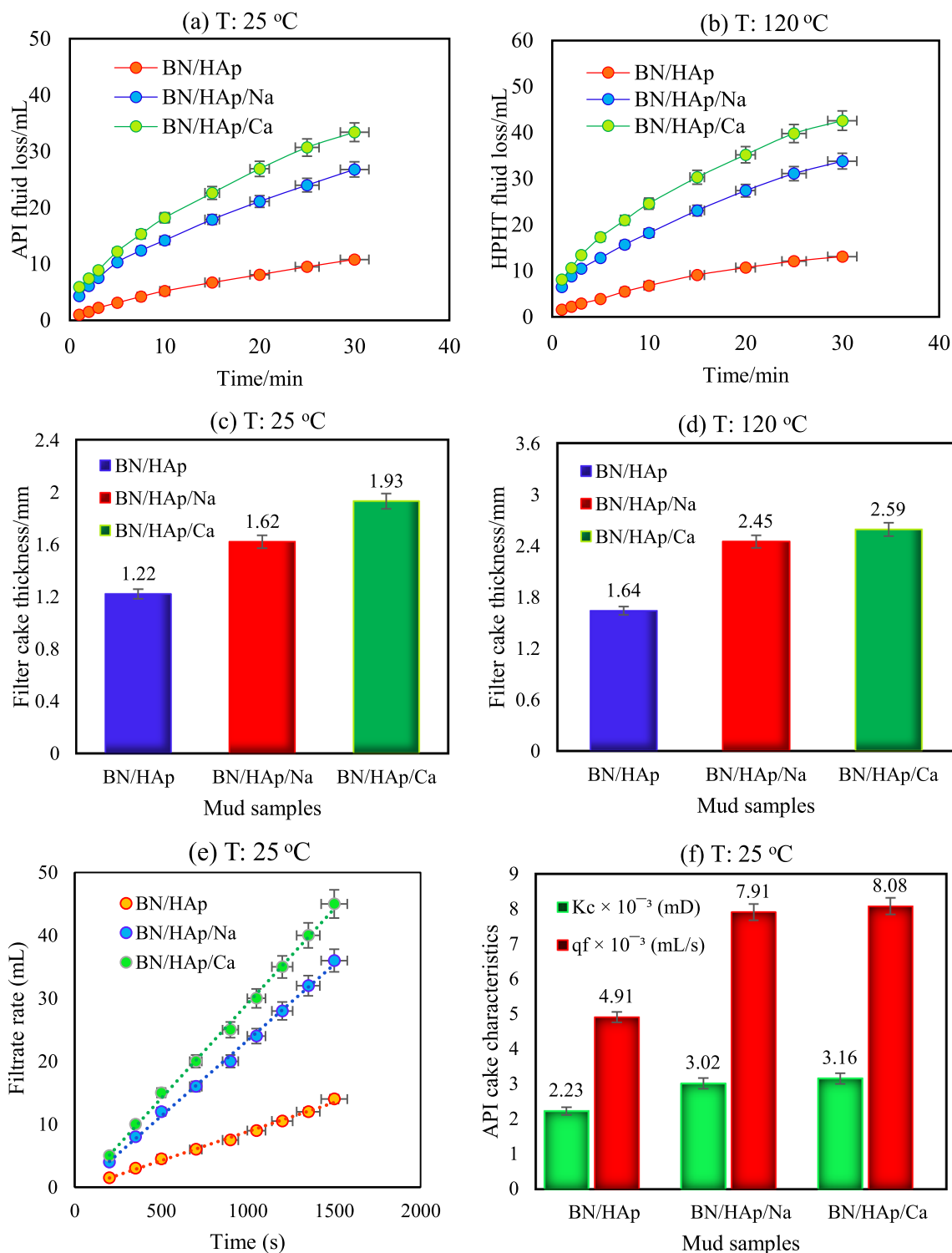


Fig. 16 BN/HAp-salt-contaminated suspension showing the values of filtration features **a** fluid loss at 25 °C; **b** fluid loss at 120 °C; **c** cake thickness at 25 °C; **d** cake thickness at 120 °C; **e** API filtration rate; and

f formed API filter cake characteristics. Note: In (e), the slopes of the dashed lines indicate the filtration rate of the precipitated filter cake

Table 7 Filtration attributes of Nano-HAp in BN-WBM at CaCl₂ and NaCl conditions

Mud sample	Temperature	Filtrate loss (mL/30 min)	%ΔFL	Cake thickness (mm/30 min)	%ΔFCT
BN/HAp	API @ 25 °C	10.8	− 50.9	1.22	− 20.3
	HPHT @ 120 °C	13.1	− 57.7	1.64	− 31.1
BN/HAp/Na	API @ 25 °C	26.8	+ 21.8	1.62	+ 5.88
	HPHT @ 120 °C	33.8	+ 9.03	2.45	+ 2.94
BN/HAp/Ca	API @ 25 °C	33.4	+ 51.8	1.93	+ 26.1
	HPHT @ 120 °C	42.6	+ 37.4	2.59	+ 8.83

4.6 Filtration Properties of Nano-HAp in BN-Based Suspension Under Salt Cations

Figure 16 depicts the filtrate loss features of the BN/HAp mud system, and Table 7 summarizes the filtration results. This finding is comparable to the rheological properties data obtained under Sect. 4.5, in which the 0.5 wt% Nano-HAp concentration considerably enhanced the viscosity stability of the BN-based water solutions without salt cations. In the presence of salt concentrations, it reduced the BN mud system's rheological values [18, 25]. At API conditions, Nano-HAp significantly reduced the BN filtrate loss volume to 10.8 mL from 22 mL (which is about a 51% reduction) (Table 7). However, after 16 h of oven ageing at 120 °C, the HPHT FL of the BN-based suspension increased to 31 mL, and it reduced to 13.1 mL with 0.5 wt% Nano-HAp (Fig. 16b). Adsorption of surface-coated Nano-HAp sulphate head groups on the edge face surfaces of BN minimized the aggregation and coalescence of BN particles and kept their dispersion and stability at 120 °C, which reduced the HPHT FL [18, 24]. The fluid loss volume under API conditions increased to 33.4 mL (by 51.8%), while that under HPHT settings increased to 42.6 mL (by 37.4%), when a CaCl₂ concentration of 5 wt% was introduced to the BN/HAp. Similar to this, with 5 wt% concentration of NaCl, the fluid loss volume of the BN/HAp mud system increased by 21.8% and 9.03% under API and HPHT conditions, respectively, to reach 26.3 mL and 33.8 mL (Table 7). Also, the BN/HAp mud cake is about 20% and 31% thinner than the BN mud cake under API and HPHT conditions, respectively. The Nano-HAp mud sample, as shown in Fig. 16c and d, formed a rigid and smooth filter cake, and the small-sized particles filled the spaces between the large BN particles to decrease the BN-based suspension filtrate loss [11].

When salt cations were present, the BN/HAp cake thickness increased slightly. But, for comparison with BN-based suspensions containing NaCl and CaCl₂ concentrations, the thickness of the formed filter cake of the mud systems of BN/HAp free of salt contamination was much lower (refer to Fig. 13c and d), illustrating the effectiveness of the particles of the SDS-aided Nano-HAp in screening the cations

of sodium and calcium. This activity aided in the reduction of filtrate loss [11, 25]. Under API conditions, for example, inclusion of the salt concentrations increased the cake thickness of the mud systems of BN/HAp by 26.1% (with CaCl₂) and 5.88% (with NaCl) (Fig. 16), as compared to the changes seen when the salts were administered to the BN-water solution without Nano-HAp (refer to Fig. 13). The API FCT was thickened by 198% and 256% with NaCl and CaCl₂ in the BN-water solution, respectively. This indicates that the Nano-HAp deposited a better-quality filter cake that efficiently screened the valence cations.

Figure 16e shows the slopes of the dashed lines of the API filtrate volume (mL) versus time (s), indicating the filtration rate of the precipitated filter cake, with the valence cations having higher filtration rates. Figure 16f displays that the concentrations of Nano-HAp at 0.5 wt% reduced the BN's API permeability and filtration rate from 0.00281 mD and 0.00772 mL/s to 0.00223 mD and 0.004910 mL/s, respectively. The addition of Nano-HAp to BN-WBM resulted in a decrease in permeability owing to the blockage of microcavities on the surface of the filter cake. These cake features of the BN/HAp mud system, however, were increased marginally with the salt cations. The permeability and filtration rate of BN/HAp with 5.0 wt% CaCl₂ are 0.00316 mD and 0.00808 mL/s, respectively. For 5.0 wt% of NaCl, the permeability and filtration rates are 0.00302 mD and 0.00791 mL/s, respectively. These two factors, respectively, increased by 12.5% and 4.7% (BN/HAp/Ca) and 7.47% and 2.46% (BN/HAp/Na), as compared to BN.

When comparing BN/Na and BN/Ca with BN-based water solutions, the increase in filtration rate and permeability is around 130% and 323.5% for BN/Na and 177% and 1063% for BN/Ca (refer: Fig. 16). The divalent Ca²⁺ ion, in comparison with the monovalent Na⁺ ion, caused higher rheology and higher water loss in the drilling mud system of BN/HAp. From the illustrations thus far, this study demonstrated that the fluid losses and rheology of BN/HAp were less salt-reliant compared to BN-based water solutions. Overall, the findings showed that the addition of Nano-HAp particles to the BN-based solution reduced the fluid loss with or without salt

concentrations, raised the viscosity without salt concentrations, and decreased the viscosity with salt concentrations, thereby ensuring safe drilling operation [9, 25]. This shows that the Nano-HAp particles successfully protected the BN platelets from salt contamination.

4.7 Salt Shielding Process of Nano-HAp in BN-Based Suspension at 25 and 120 °C

The divalent Ca^{2+} and monovalent Na^+ inorganic salts introduced created shear-induced aggregated and flocculated BN structure, respectively, symbolizing the salt-contamination process in BN. Figure 17 depicts the salt shielding process of BN by the particles of Nano-HAp, which resulted in decreased BN viscosity and fluid loss. Figure 17b shows how the “bridge” function of negatively charged Nano-HAp-linked BN platelets is achieved by “edge-face (Fig. 17a) and edge-edge (Fig. 17c)” attachment, resulting in hindering aggregation and flocculation and thereby forming a rigid network structure of BN particles [18, 20, 24, 25]. The addition of Nano-HAp concentration of 0.5 wt% (Fig. 17b) to the BN-based water solution caused the negatively charged Nano-HAp particles to electrostatically attach to the edge surfaces of BN particles having positive charges (Fig. 17c), increasing the suspension viscosity. Due to their high electrostatic attraction, the particles of Nano-HAp carrying negative charges adsorbed physically on the face surfaces of the particles of BN via the negatively charged BN platelet surface (Fig. 17a). This hindered aggregation and reduce the loss of drilling fluid by shielding the BN platelet-face surface [9, 11].

During the shielding of the Na^+ cations from the BN platelets, the particles of Nano-HAp prevented the Na^+ ions from interacting with the platelets of BN (Fig. 17c) [25]. Similar to how the Na^+ cations were protected from the platelets of BN, the divalent cations (Ca^{2+}) remained attached to the platelets of BN via a “face-edge” mode and were shielded from the BN platelets (Fig. 17a). These mechanisms reduced the fluid loss and viscosity parameters of BN-based water solutions with salt concentrations and prevented the flocculation and aggregation of BN, respectively, caused by the cations of sodium and calcium [11, 18]. Dispersion, hydration, and flocculation of BN platelets are all affected by the ionic strength of the surrounding water [11, 18, 25]. When Nano-HAp was added to water-BN-based solutions holding salt ions, the concentration of salt rose while the hydration and dispersion rates declined. This happens because the exchange cations are brought nearer to the particles surface of BN [21, 24, 49]. This weakens the bond between the exchange cations and the BN surface by reducing the thickness of the water layer. Therefore, both filtrate loss and rheological parameters are reduced.

According to these findings, the results support the hypothesis that decreasing the filtrate loss and controlling the viscosity of BN-water solutions in the face of salt contamination requires protecting both the face and edge surfaces of BN platelets. This act will not only avoid BN-salt engagement but will also hinder the development of BN particle flocculation and aggregation [9]. Under Ca^{2+} and Na^+ conditions, Nano-HAp was able to maintain and enhance BN dispersion while inhibiting BN platelet aggregation and flocculation, therefore hindering the salt cations from contaminating the BN platelets and preserving the BN plate-shaped structure. This mechanism improved the performance of BN-based suspensions in the presence of CaCl_2 and NaCl contamination, making them suitable for deep and ultra-deep well drilling.

5 High-Temperature (150–210 °C) Effects on SDS-Assisted Nano-HAp Particles in BN-Based Water Systems Under CaCl_2 and NaCl Contamination

During the drilling of extreme-temperature deep and ultra-deep wells, encountering hydratable cations (Ca^{2+} and Na^+) that can easily contaminate the drilling mud could be inevitable. These cations can degrade the drilling mud’s filtration control and rheological performance. Therefore, after 16 h of ageing at 150, 180, and 210 °C, the filtration and rheological performance of Nano-HAp in BN-WBMs under CaCl_2 and NaCl contaminants were assessed, and the experimental findings are reported under this section.

5.1 Viscosity Effect Between 150 and 210 °C

Drilling fluids must have sufficient rheological features to transport and suspend drilled cuttings and preserve well-bore stability, particularly in deep and ultra-deep wells where high temperatures and salt contamination are expected. Thus, Fig. 18 and Table 8 show the viscosity of BN-based solutions containing 0.5 wt% Nano-HAp under salt contamination at 150, 180, and 210 °C. As demonstrated in Fig. 18a–c, a 0.5 wt% Nano-HAp concentration increased the viscosities of a 4.8 wt% BN concentration of 4.01, 3.71, and 1.55 mPa s at 150, 180, and 210 °C, to 8.23, 8.07, and 6.43 mPa s at a shear rate of 1022 s^{-1} , respectively. In Fig. 18a–c, viscosities decrease with increasing temperature. BN particles in aqueous solution will aggregate and flocculate under CaCl_2 and NaCl assault at high temperatures, decreasing viscosity [25]. NaCl and CaCl_2 increased the BN suspension viscosity by 1072–1326% and 1325–1596% at a 1022 s^{-1} shear rate between 150 and 210 °C, respectively. Thus, between 150 and 210 °C, NaCl and CaCl_2 increase BN suspension viscosities by 12–14-fold and 14–17-fold, respectively. Salt

Fig. 17 Nano-HAp mechanism in protecting BN platelets from salt cation attack: **a** calcium cations; **b** Nano-HAp anions; and **c** sodium cations. The yellow/red plate stands for the Nano-HAp (yellow is the SDS layer), whereas the blue/ash plate denotes BN platelets

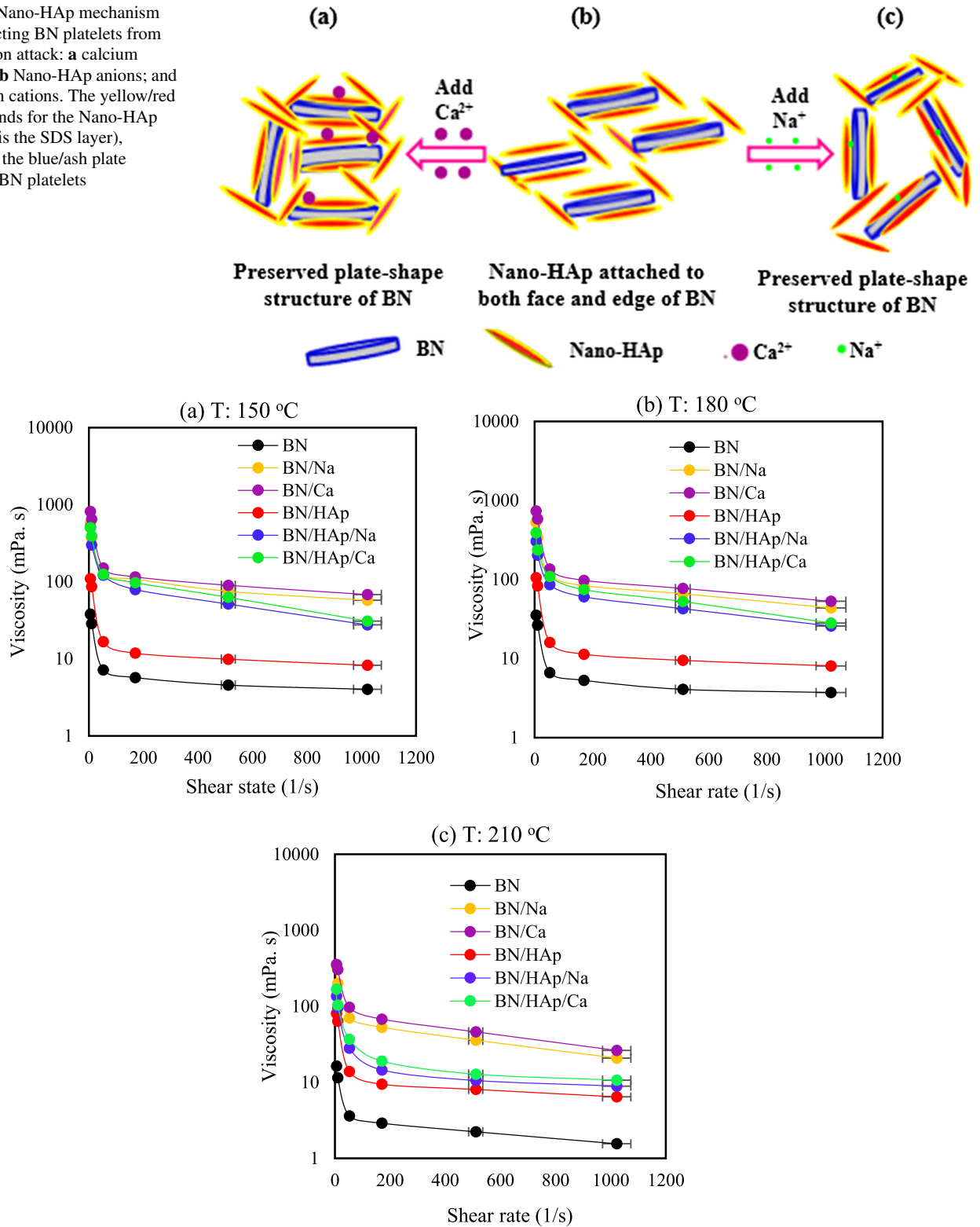


Fig. 18 Effect of Nano-HAp in BN-based suspension under NaCl and CaCl₂ contamination at high temperatures: **a** 150 °C, **b** 180 °C, and **c** 210 °C

Table 8 High temperatures viscosity behaviour of Nano-HAp in BN-based suspension under CaCl₂ and NaCl contamination

Drilling muds	% Change in viscosity from 25–210 °C at 1022 s ⁻¹ shear rate					
	25–150 °C	25–180 °C	25–210 °C	%Δμ @ 150 °C	%Δμ @ 180 °C	%Δμ @ 210 °C
BN	27.1	32.5	71.8	–	–	–
BN/Na	49.4	61.6	81.6	1326% increase	1072% increase	1242% increase
BN/Ca	56.2	66.5	83.1	1596% increase	1325% increase	1590% increase
BN/HAp	17.7	19.3	35.7	105% increase	118% increase	315% increase
BN/HAp/Na	31.3	35.7	77.8	586% increase	593% increase	474% increase
BN/HAp/Ca	38.6	43.8	78.6	666% increase	657% increase	590% increase

cations greatly impact the dispersion, hydration, and flocculation of colloidal BN suspension, causing inappropriate viscosity values that might cause large frictional pressure losses and excessive pump load during mud circulation [6, 36].

At a shear rate of 1022 s⁻¹, BN-based suspension viscosity increased by 105–315% between 150 and 210 °C when the concentration of Nano-HAp at 0.5 wt% was used (Fig. 18a–c and Table 8). Furthermore, with the 0.5 wt% Nano-HAp, the BN-based suspension under 5 wt% NaCl or CaCl₂ cation attack recovers greatly. Between 150 and 210 °C, BN/HAp with CaCl₂ contamination increased its viscosity by 590–666%, whereas BN/HAp viscosity under NaCl conditions increased by 474–586%. This implies that at 210 °C, the viscosities of BN-based solutions containing NaCl and CaCl₂ concentrations were reduced by 134% and 146%, respectively, with the addition of 0.5 wt% Nano-HAp. The anionic SDS provides a hydrophilic sulphate head group for strong hydration that is not susceptible to external metal cations and high-temperature attacks, increasing the thermal stability and salt resistance of the SDS-assisted Nano-HAp [9, 25]. When the inorganic salts were introduced into the drilling mud systems of BN containing Nano-HAp, Nano-HAp adsorbed on the BN particles and shielded the sodium and calcium cations from the platelets of BN. Consequently, the face-to-face coalescence and aggregation and edge-to-face flocculation of BN were minimized at high temperatures, and the dispersion of BN particles was promoted, resulting in a lower fluid system suspension viscosity [21, 24].

The drilling mud of BN/HAp only degrades by 35.7% at 210 °C after 16 h of ageing, while the BN-based suspension and BN suspension under salt contamination degrade by < 72% and < 84%, respectively. At 210 °C, the BN/HAp-based suspension's viscosity deterioration increased by about 79% under inorganic salt concentrations, demonstrating that the particles are still vulnerable to salt cation contamination.

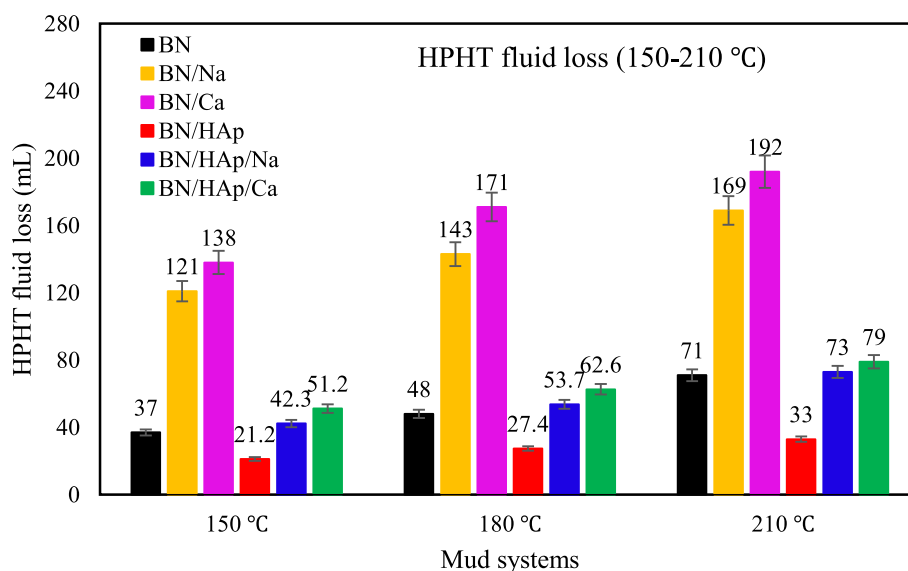
Furthermore, the viscosity deterioration related to the mud system of BN/HAp containing the NaCl and CaCl contamination is tolerable at 150 and 180 °C when compared to the BN-based solution with inorganic salts. This suggests that in a freshwater mud, salt-contaminated drilling muds will minimize the pressure needed to move drilled cuttings from the well's bottom to its annulus and back to the surface [25]. The Nano-HAp kept the solid particles in BN-salt-contaminated solutions well dispersed, inhibited BN aggregation and passivation at high temperatures, minimized solid particle friction, and reduced the viscosity [4].

5.2 Fluid Loss Control Effect Between 150 and 210 °C

A fundamental drilling fluid challenge at high temperatures is controlling and stabilizing mud properties under severe surface-to-bottomhole temperature variations. Rapid temperature fluctuations have an impact on fluid filtration control and drilling performance [3, 19]. Figure 19 depicts the filtrate loss volume of the mud system of Nano-HAp when subjected to salt cation attack and at temperatures ranging from 150 to 210 °C. Except for Nano-HAp, which only permits 33 mL after 30 min of filtration at 210 °C, the fluid loss of all the mud samples following high-temperature ageing showed a rapid rising trend. The BN had a minimum fluid loss of 37 and 48 mL at 150 and 180 °C, respectively, while the fluid loss rose dramatically to 71 mL at 210 °C. This is because high temperatures exacerbated BN particle dehydration, aggregation, flocculation, and coalescence, increasing BN particle size, lowering BN suspension viscosity, leading to substantial filtrate loss [4, 24, 25]. The fluid loss of the BN was reduced by 42.7%, 42.9%, and 53.5% at 150, 180, and 210 °C, respectively, with Nano-HAp demonstrating effective fluid loss management. This was mostly due to the Nano-HAp's outstanding temperature resistance (see Fig. 6), high adsorption capacity, smaller size, and good



Fig. 19 Effect of high temperatures on the fluid loss of Nano-HAp in BN-salt WBM



hydration characteristics. The thermal and dispersion stability of the BN particles was enhanced, and smaller Nano-HAp particles occupied the pore spaces between the larger BN particles to prevent fluid loss [39].

When inorganic salts were introduced, the effects of high temperatures on the BN solution were amplified. Between 150 and 210 °C, the fluid loss of the BN increased by 138–227% with NaCl concentration and 170–273% with CaCl₂ concentration, confirming that hydratable salt cations have a substantial unfavourable influence on the filtration characteristics of the drilling fluids. This is because salt cations can decrease the electrostatic repulsion between BN particles, resulting in aggregation or flocculation of BN and a decrease in hydration and dispersion capacity [22, 25]. Furthermore, inorganic salt ionic concentration can affect the charge distribution at the BN edge face surfaces, leading to flocculation, increased viscosity, and increased fluid loss [21]. However, the fluid loss of the BN-based suspensions under salt contamination and high temperatures was reduced by 59–63% with CaCl₂ and 57–65% with NaCl when the concentration of Nano-HAp at 0.5 wt% was introduced between 150 and 210 °C. When comparing the effects of the cations of calcium and sodium investigated on BN-water solutions, it was found that NaCl cations exhibited the least negative impact on viscosity and fluid loss. In general, the findings from previous studies on the effects of inorganic salts on WBM characteristics are similar to this study's findings [9, 20, 21]. In these studies, adding inorganic salts unduly increased the viscosity and fluid loss volume of the drilling fluid systems, and a low concentration of the treated fluid additive between 0.1 and 1.0 wt% significantly decreased these properties. In this study, BN-based water solutions under salt contamination had decreased viscosity and filtrate loss with 0.5 wt% Nano-HAp. Overall, salt cations produced

BN particle aggregation and flocculation. Divalent cations contaminated the BN layers more severely and caused BN particle aggregation than did NaCl, which has a lower cation replacement capacity. This finding is also comparable to those of previous studies [9, 20, 21], in which the detrimental effect of BN-based water solutions was greater with divalent cations (CaCl₂) than with monovalent cations (NaCl). The newly-developed SDS-assisted Nano-HAp exhibited good filtration control capacity under the evaluated temperatures and salt conditions, indicating its potential for applications in deep and ultra-deep well drilling.

5.3 Filter Cake Thickness and SEM Analysis of Filter Cake Surface

To avoid blowout mishaps while drilling, the water column pressure of the drilling fluids must be slightly higher than the pressure of the formation to ensure that the drilling mud particles in solid state accumulate on the borehole and create a thin film of filter cake. The filter cake quality influences not just the loss of water but also the borehole stability and reservoir preservation [24]. The ideal filter cake ought to possess a firm and dense nature with few leaking pores to prevent water from seeping into the formation. To assess the filtration control capacity of the Nano-HAp, it is required to use SEM to investigate the impact on the morphology of the filter cake. Previous research that examined the morphology of filter cakes generated by water-BN suspensions emphasized that the homogeneity of the filter cake in structure and composition influences the properties of the filtration process of drilling fluid [2, 50, 51].

This section focuses on comprehending the composition of the different filter cakes formed by drilling fluids in non-reservoir sections to verify the improvement in properties of

Table 9 Filter cake's thickness (mm) from 150 to 210 °C

Drilling muds	HPHT FL (mm) from (150–210 °C)		
	150 °C	180 °C	210 °C
BN	2.39	2.40	2.63
BN/Na	4.76	4.79	5.11
BN/Ca	5.74	5.77	5.94
BN/HAp	1.91	2.31	2.53
BN/HAp/Na	2.43	2.47	2.64
BN/HAp/Ca	2.51	2.55	2.72

BN-WBM containing Nano-HAp. As a result, SEM investigation of the dried filter cake's surface morphology was performed, according to previous studies [50, 51]. The filter cakes were produced after a 30-min filtration test at a heating jacket temperature of 210 °C and 500 psi differential pressure. The filter cakes were subjected to ambient temperature (~ 25 °C) conditions and dried using the natural air-drying approach without using any kind of oven or other drying apparatus. The drying process showed that a duration of 4 days was required for the filter cakes to achieve full dryness. The dried filter cakes were cut into thinner bits with a razor blade, and these pieces were subsequently taped with carbon to a SEM stub. Before the filter cakes were analysed with a SEM SU8020 that has an electron-accelerating voltage of 5.0 kV, they were coated with 4 nm of gold using a Leica EM ACE600 sputter coater. Table 9 shows the filter cake thickness findings of all the mud samples at temperatures of 150, 180, and 210 °C, and it demonstrates that the thickness of the cakes increased with increasing temperature. According to Table 9, adding inorganic salts substantially doubled the thickness of BN-based suspension filter cakes. A BN-salt-contaminated solution with Nano-HAp concentration of 0.5 wt% minimally raised the filter cake thickness.

Figure 20 displays images of the filter cake surface morphology under SEM analysis. The images were captured inside a plane that is perpendicular to the flow plane of the filter cakes. This was done to identify any changes in the chemical composition of the filter cakes at a micro-structural level [50]. The filter cake of the BN-based solution (Fig. 20a) is thin, dense, and smooth, and the SEM image showed that BN has a stacked layer with a few porous structure that enabled fluid loss of 71 mL (Fig. 20) and cake thickness of 2.63 mm. This is because the high temperature exacerbated the BN filter cake's tendency to aggregate, which reduced the filter cake's quality [51]. As illustrated in Fig. 20b and c, adding NaCl or CaCl₂ to the BN-based solution thickens the filter cake and creates small pores. This reduces the filter cake's water-blocking capacity. Thus, larger drilling fluid (water) leaks through the filter cakes compared to BN. High

temperatures and salt cations (Ca²⁺ and Na⁺) worsened BN particle aggregation and flocculation in the BN-water solution, increasing the filter cake porosity and making filtrate blocking difficult [50]. The significant filtrate loss volume in BN/Na and BN/Ca mud systems (Fig. 18) supports this conclusion. BN-water solutions under salt cation attack showed comparable filter cake surface morphology with previous studies [18, 50, 51].

According to Fig. 20d, the BN-based solution containing Nano-HAp produced a thin, smooth, uniform, and dense filter cake of 2.53 mm with few leakage pores, demonstrating that Nano-HAp improved the BN filter cake quality. A thin, low-permeable, and dense filter cake aids drilling and strengthens the wellbore, but thick ones may cause blocked pipes, drag, torque and excessive surge and swab pressures [24]. Adding CaCl₂ or NaCl to the BN/HAp-based solutions made the filter cakes thinner (Fig. 20e and f) than the filter cakes without Nano-HAp (Fig. 20b and c), and the SEM images of Fig. 20e and f revealed no evident drilling mud aggregation or agglomeration but few leakage pores. Based on this finding, high temperatures modify the filter cakes' properties under salt cation assault. Also, after ageing, Nano-HAp still displayed strong adsorption ability, inhibiting coalescence and aggregation and increasing the temperature and salt resistance of BN-based suspensions, thus improving the filter cake quality.

5.4 Zeta Potential of BN-Based Solutions Containing Both Nano-HAp and Salt Contamination

The zeta potential is a crucial metric for characterizing colloidal stability in WBM, which is an intricately thermally unstable dispersion of colloidal particles. The zeta potential, particle dispersion, and colloidal stability will all increase with increasing electric double layer thickness [52]. Zeta potential analyses were used to examine the impact of the Nano-HAp particles on the BN particles stability and dispersion. The zeta potential of a BN-water solution containing a concentration of Nano-HAp at 0.5 wt% was measured both before and after ageing, with the findings shown in Fig. 21. The findings demonstrate that all the drilling muds experience a decline in absolute zeta potential after 210 °C ageing, indicating that high temperature exacerbates the thermal transport of water molecules, which in turn thins the BN hydration film layer, supports particle coalescence, weakens dispersibility, and impairs stability [21, 22]. The BN particle's colloidal stability was compromised by high-temperature ageing, which increased its negative charge and caused a decrease in its absolute zeta potential from 32 mV (25 °C) to 21 mV (210 °C).

The absolute value of the zeta potential distinctly increases towards the less negative stable region before (40 mV) and after ageing (38 mV) after adding Nano-HAp because it is adsorbed on BN particles, thickening the diffusion

Fig. 20 SEM images of filter cakes top surface of BN-based suspensions aged at 210 °C: **a** 4.8 wt% BN, **b** 5 wt% NaCl, **c** 5 wt% CaCl₂, **d** 0.5 wt% Nano-HAp, **e** 0.5 wt% Nano-HAp and 5 wt% NaCl, and **f** 0.5 wt% Nano-HAp and 5 wt% CaCl₂ concentrations

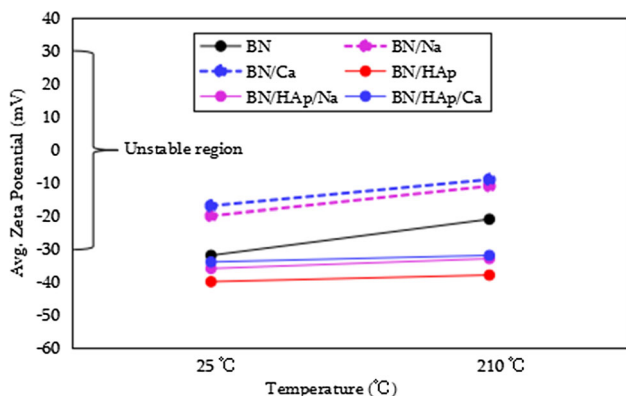
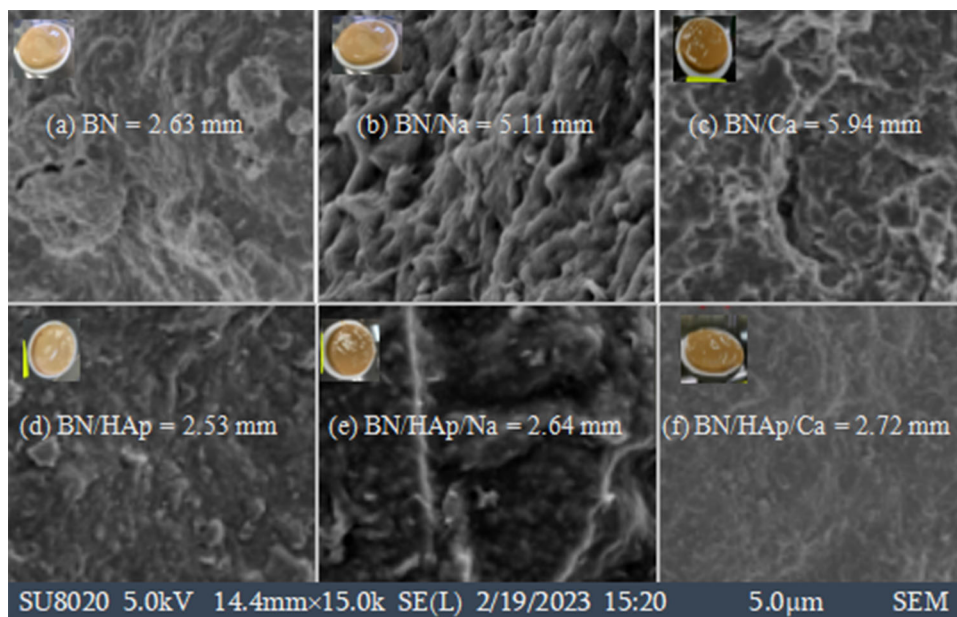


Fig. 21 Zeta potential of drilling muds

double layer, preventing BN coalescence, and improving its stability [2, 9]. When CaCl₂ and NaCl were added to BN-water solutions, the diffusion double layer of the BN compressed, causing the absolute value of the zeta potential to decrease dramatically towards the more negative unstable region (between 9 and 20 mV). Furthermore, when Ca²⁺ and Na⁺ penetrate the BN surface, electrostatic shielding occurs, reducing the repulsive force between BN particles and decreasing their stability [25, 50]. Given that Nano-HAp is adsorbed on BN particles to prevent BN coalescence, and some Ca²⁺ and Na⁺ pervade into the molecular chain of Nano-HAp, further impeding BN particle aggregation and flocculation, the absolute value of the zeta potential rises sharply towards the less negative stable region (between 32 and 36 mV), improving stability [2, 25].

The zeta potential values of the drilling muds containing SDS-assisted Nano-HAp and CaCl₂ and NaCl reveal that the

drilling muds have an optimal zeta potential in a BN-saturated salt solution and after 210 °C ageing. Overall, this finding indicates that Nano-HAp particles could be useful for the enhancement of the filtration characteristics and rheological parameters of drilling muds contaminated with salt cations when aged at high temperatures up to 210 °C. It can improve BN suspension stability and dispersion in high-temperature and electrolyte solutions, potentially facilitating drilling in deep and ultra-deep formations.

6 The Study's Implications and Potential Cost Feasibility of Nano-HAp

Based on the study's findings, the implications of this study are that the developed Nano-HAp particles have the potential to improve the properties of drilling fluids and minimize the effect of salt cations in salty drilling fluids. The TGA revealed that Nano-HAp has exceptional thermal stability. The degradation temperature of the evaluated Nano-HAp (refer to Fig. 6) was up to 750 °C (with only approximately 27% weight loss), indicating its potential for use in high-temperature wells. Thus, it showed beneficial and promising attributes at high temperatures under CaCl₂ and NaCl conditions. It can form a good dispersion, and it possesses the desirable viscosity needed to improve cutting transport and hole cleaning due to the hydrophilic head groups of SDS. Furthermore, it efficiently decreased the fluid loss of BN-water solutions and significantly controlled the excessive fluid loss volume of the salt-contaminated drilling muds. These attributes can prevent fine migration, formation damage, wettability alteration, and increase the efficiency of drilling

fluids. Moreover, the good fluid loss control attribute can make the Nano-HAp drill effectively in water-sensitive shale formation to inhibit shale swelling and dispersion through the hydrophobic tail of SDS. However, Nano-HAp performance can be strongly dependent on its precursors, modifications, and preparation methods for efficient dispersion and stability. A highly dispersed and thermally stable prepared Nano-HAp will have the potential to perform optimally in drilling fluids and to improve the drilling process.

Additionally, calcium phosphate, a naturally occurring mineral with significant biological, chemical, and agricultural applications, is present in Nano-HAp. Through the calcination process, it may be derived from natural sources such as fish bone, beef bone, coral, sea shells, and egg shells [32, 38]. It is also economically viable since calcium-phosphate-containing waste streams may be treated to recover it [32]. The synthesized Nano-HAp has been found to be cost-effective [32] and is mostly made up of calcium- and phosphate-containing naturally occurring minerals. Given that the components are more affordable, non-toxic, and easy to synthesize, the in situ precipitation approach used to synthesize Nano-HAp has special benefits [32, 33]. Additionally, with a controlled size and form of HAp, the resultant biocompatible product may be applied to human bones [38]. In this work, 0.5 wt% of Nano-HAp was added to 350 mL of drilling mud, which, at this very low concentration, showed outstanding fluid characteristics. This inevitably suggests that its field use could require a low concentration to work best, making it economically viable to produce Nano-HAp on a large scale for field applications.

7 Conclusions

This research shows how Nano-HAp was synthesized through an in situ chemical precipitation method with the aid of SDS, characterized, and applied in BN-WBMs where salt contamination exists at temperatures of 25, 120, 150, 180, and 210 °C. A BN-salt-contaminated water solution was prepared with 4.8 wt% BN and 5 wt% each of NaCl and CaCl₂, and the rheological and filtration properties were measured. 0.5 wt% Nano-HAp was added to the solution to determine its salt resistance and response to high temperatures. The key points of this study, based on the results and goals met, are itemized as follows:

- 0.5 wt% of Nano-HAp decreased the amount of fluid loss of 4.8 wt% BN in water solution from 22 to 10.8 mL by 51% (API settings) and from 71 to 33 mL by 53.5% (HPHT settings).
- After 16 h of ageing at 210 °C, the BN platelets were very susceptible to Ca²⁺/Na⁺ assaults, resulting in high aggregation, coalescence, and flocculation of the BN-WBMs. At a shear rate of 1022 s⁻¹, the viscosity of BN disproportionately increased with NaCl, from 1.553 to 8.91 mPa.s by 1242%, and it increased even more with CaCl₂, from 1.553 to 10.67 mPa s by 1590%.
- However, Nano-HAp particles remarkably reduced the salt-sensitive viscosity and fluid loss of BN-WBMs under salt cation assault at all temperatures. For example, for a shear rate of 1022 s⁻¹ at 210 °C, it decreased the viscosity of BN/Ca from 26.23 to 10.67 mPa s by 59% and fluid loss from 192 to 79 mL by 59%, by protecting the positive edge and negative face surfaces of BN platelets.
- NaCl salt generally has the least detrimental effects on the rheological and filtration characteristics of BN-WBMs, while CaCl₂ offers the most severe environment. Salts may have an adverse impact on the rheological and filtration characteristics of bentonite dispersion in drilling operations.
- Overall, Nano-HAp greatly improves the salt and temperature resistance of BN-WBM and makes the drilling mud more efficient in high-salinity, high-temperature environments. These characteristics will improve deep and ultra-deep well drilling or drilling offshore to improve the drilling process. This increased global demands for oil and gas.

Acknowledgements The authors would like to acknowledge the financial support from the Ministry of Higher Education, Malaysia, under the Fundamental Research Grant Scheme (FRGS) via reference number FRGS/PV/2022/03075 and Universiti Teknologi Malaysia for the funding under UTM Fundamental Research (UTMFR) (Q.J130000.21A2.06E09) and the Fundamental Research Grant Scheme (FRGS) (Ref: FRGS/1/2021/TK0/UTM/02/73, FRGS/1/2023/TK09/UTM/02/13). Engr. Dr. Jeffrey Onuoma Oseh is a researcher at UTM under the postdoctoral fellowship scheme for the project "Evaluation of Modified Hydroxyapatite Nanoparticles for Rheological and Filtration Properties Modification in Field-Applicable Drilling Muds".

Authors contributions Conceptualization: J.O. Oseh and M.N.A.M. Norddin; Methodology: J.O. Oseh and E.N. Ngouangna; Formal analysis: J.O. Oseh; Investigation: J.O. Oseh and M.N. Yahya; Resources: M.N.A.M. Norddin and I. Ismail; Data curation: J.O. Oseh; Writing-original draft preparation: J.O. Oseh and A.O. Gbadamosi; Writing-review and editing: J.O. Oseh, A. Agi, and U.I. Duru; Funding acquisition: M.N.A.M. Norddin and A.R. Risal. All the authors have read and approved the published version of this research.

Declarations

Conflict of interest All the authors have read and approved the published version of this research with no conflicts of interest. The authors (J.O. Oseh, M.N.A.M. Norddin, A.O. Gbadamosi, I. Ismail, E.N. Ngouangna, U.I. Duru, A.R. Risal, M.N. Yahya, and A. Agi) declare that they have no known competing financial interests or personal relationships that could have appeared to influence the work reported in this manuscript.



References

- Guo, X.; Hu, D.; Li, Y.; Duan, J.; Zhang, X.; Fan, X.; Duan, H.; Li, W.: Theoretical progress and key technologies of onshore ultra-deep oil/gas exploration. *Engineering* **5**, 458–470 (2019)
- Liu, J.; Zhang, X.; Zhang, W.; Lv, K.; Bai, Y.; Wang, J.; Huang, X.; Jin, J.; Sun, J.: Carbon nanotube enhanced water-based drilling fluid for high temperature and high salinity deep resource development. *Pet. Sci.* **19**, 916–926 (2021)
- Sun, J.; Zhang, X.; Lv, K.; Liu, J.; Xiu, Z.; Wang, X.; Huang, X.; Bai, Y.; Wang, J.; Jin, J.: Synthesis of hydrophobic associative polymers to improve the rheological and filtration performance of drilling fluids under high temperature and high salinity conditions. *J. Pet. Sci. Eng.* **209**, 109808 (2022)
- Li, J.; Sun, J.; Lv, K.; Ji, Y.; Liu, J.; Huang, X.; Bai, Y.; Wang, J.; Jin, J.; Shi, S.: Temperature- and salt-resistant micro-crosslinked polyampholyte gel as fluid-loss additive for water-based drilling fluids. *Gels* **8**, 289 (2022)
- Liu, J.; Dai, Z.; Xu, K.; Yang, Y.; Lv, K.; Huang, X.; Sun, J.: Water-based drilling fluid containing bentonite/poly(sodium 4-styrene sulfonate) composite for ultra-high temperature ultra-deep drilling and its field performance. *SPE J.* **25**, 1193–1203 (2020)
- Medhi, S.; Gupta, D.K.; Sangwai, J.S.: Impact of zinc oxide nanoparticles on the rheological and fluid-loss properties, and the hydraulic performance of nondamaging drilling fluid. *J. Nat. Gas Sci. Eng.* **88**, 103834 (2021). <https://doi.org/10.1016/j.jngse.2021.103834>
- Bello, A.; Ivanova, A.; Cheremisin, A.: Enhancing N₂ and CO₂ foam stability by surfactants and nanoparticles at high temperature and various salinities. *J. Pet. Sci. Eng.* **215**, 110720 (2022). <https://doi.org/10.1016/j.petrol.2022.110720>
- Ivanova, A.A.; Phan, C.; Barifcani, A.; Iglauer, S.; Cheremisin, A.N.: Effect of nanoparticles on viscosity and interfacial tension of aqueous surfactant solutions at high salinity and high temperature. *J. Surfactants Deterg.* **23**, 327–338 (2019)
- Zhu, W.; Zheng, X.; Shi, J.; Wang, Y.: A high-temperature resistant colloid gas aphron drilling fluid system prepared by using a novel graft copolymer xanthan gum-AA/AM/AMPS. *J. Pet. Sci. Eng.* **205**, 108821 (2021)
- Sun, J.; Chang, X.; Zhang, F.; Bai, Y.; Lv, K.; Wang, J.; Zhou, X.; Wang, B.: Salt-responsive zwitterionic polymer brush based on modified silica nanoparticles as a fluid-loss additive in water-based drilling fluids. *Energy Fuels* **34**, 1669–1679 (2020)
- Balding, P.; Li, M.; Wu, Q.; Volkovinsky, R.; Russo, P.: Cellulose nanocrystal-polyelectrolyte hybrids for bentonite water based drilling fluids. *ACS Appl. Bio Mater.* **3**, 3015–3027 (2020)
- Plank, J.P.: Water-based muds using synthetic polymers developed for high temperature drilling. *Oil Gas J.* **90**, 9 (1992)
- Al-Shargabi, M.; Davoodi, S.; Wood, D.A.; Al-Musai, A.; Rukavishnikov, V.S.; Minaev, K.M.: Nanoparticle applications as beneficial oil and gas drilling fluid additives: a review. *J. Mol. Liq.* **352**, 118725 (2022)
- Beg, O.A.; Espinoza, D.E.S.; Kadir, A.; Shamshuddin, M.; Sohail, A.: Experimental study of improved rheology and lubricity of drilling fluids enhanced with nanoparticles. *Appl. Nanosci.* **8**, 1069–1090 (2018)
- Wu, Y.; Wang, Z.; Yan, Z.; Zhang, T.; Bai, Y.; Wang, P.; Luo, P.; Gou, S.; Guo, Q.: Poly(2-acrylamide-2-methylpropanesulfonic acid)-modified SiO₂ nanoparticles for water-based muds. *Ind. Eng. Chem. Res.* **56**, 168–174 (2017)
- Ngouangna, E.N.; Jaafar, M.D.; Norddin, M.N.A.M.; Augustine, A.; Risal, A.R.; Mamah, S.C.; Oseh, J.O.: The effect of hydroxyapatite nanoparticles on wettability and brine-oil interfacial tension as enhance oil recovery mechanisms. *J. Pet. Sci. Eng.* **218**, 110941 (2022)
- Gbadamosi, A.O.; Junin, R.; Abdalla, Y.; Agi, A.; Oseh, J.O.: Experimental investigation of the effects of silica nanoparticles on hole cleaning efficiency of water-based drilling mud. *J. Pet. Sci. Eng.* **172**, 1226–1230 (2018)
- Rezaei, A.; Nooripoor, V.; Shahbazi, K.: Applicability of Fe₃O₄ nanoparticles for improving rheological and filtration properties of bentonite-water drilling fluids in the presence of sodium, calcium, and magnesium chlorides. *J. Pet. Explor. Prod. Technol.* **10**, 2453–2464 (2020). <https://doi.org/10.1007/s13202-020-00920-6>
- Sun, Y.; Sun, J.; Li, L.; Lv, K.; Zhang, X.; Wang, Z.; Dai, Z.; Xu, Z.; Zhang, T.; Liu, J.: Development of high-temperature and high-mineralization-resistant adaptive plugging agent and its performance evaluation. *Energy Fuels* **37**(13), 8999–9010 (2023)
- Liu, F.; Jiang, G.; Peng, S.; He, Y.; Wang, J.: Amphoteric copolymer as an Anti-calcium contamination fluid-loss additive in water-based drilling fluids. *Energy Fuels* **30**, 7221–7228 (2016)
- Li, M.; Wu, Q.; Han, J.; Mei, C.; Lei, T.; Lee, S.; Gwon, J.: Overcoming salt contamination of bentonite water-based drilling fluids with blended dual functionalized cellulose nanocrystals. *ACS Sustain. Chem. Eng.* **8**, 11569–11578 (2020)
- Zhu, W.; Zheng, X.: Effective modified xanthan gum fluid loss agent for high-temperature water-based drilling fluid and the filtration control mechanism. *ACS Omega* **6**(37), 23788–23801 (2021)
- Yang, L.; Jiang, G.; Shi, Y.; Lin, X.; Yang, X.: Application of ionic liquid to a high-performance calcium-resistant additive for filtration control of bentonite/water-based drilling fluids. *J. Mater. Sci.* **52**, 6362–6375 (2017)
- Ghaderi, S.; Ramazani, A.; Haddadi, A.: Applications of highly salt and highly temperature resistance terpolymer of acrylamide/styrene/maleic anhydride monomers as a rheological modifier: rheological and corrosion protection properties studies. *J. Mol. Liq.* **294**, 111635 (2019)
- Raheem, A.M.; Vipulanandan, C.: Salt contamination and temperature impacts on the rheological and electrical resistivity behaviors of water based drilling mud. *Energy Sources Part A Recov. Util. Environ. Eff.* **42**(3), 344–364 (2020)
- Hassiba, K.J.; Amani, M.: The effect of salinity on the rheological properties of water based mud under high pressures and high temperatures for drilling offshore and deep wells. *Earth Sci. Res.* **2**(1), 175–186 (2012). <https://doi.org/10.5539/esr.v2n1p175>
- Akpan, E.U.; Enyi, G.C.; Nasr, G.G.: Enhancing the performance of xanthan gum in water-based mud systems using an environmentally friendly biopolymer. *J. Pet. Explor. Prod. Technol.* **10**, 1933–1948 (2020). <https://doi.org/10.1007/s13202-020-00837-0>
- Sami, N.A.: Effect of magnesium salt contamination on the behavior of drilling fluids. *Egypt. J. Pet.* **25**(4), 453–458 (2016). <https://doi.org/10.1016/j.ejpe.2015.10.011>
- Prasad, P.S.; Marupalli, B.C.G.; Das, S.; Das, K.: Surfactant-assisted synthesis of hydroxyapatite particles: a comprehensive review. *J. Mater. Sci.* **58**, 6076–6105 (2023)
- Nakagawa, K.; Arai, Y.; Umezaki, Y.; Yoshida, A.; Kajiwara, Y.; Aoyagi, S.; Matsuyama, H.; Sugiyama, S.: Template effect of phosphate surfactant on formation of hydroxyapatite nanostructures with various shapes. *Mater. Chem. Phys.* **213**, 183–190 (2018)
- Bulina, N.V.; Makarova, S.V.; Baev, S.G.; Matvienko, A.A.; Gerasimov, K.B.; Logutenko, O.A.; Bystrov, V.S.: A study of thermal stability of hydroxyapatite. *Minerals* **11**, 310 (2021). <https://doi.org/10.3390/min11121310>
- Annisa, T.; Azkiya, A.; Fauzi, R.N.; Nandiyanto, A.B.D.; Hofifah, S.N.: Cost analysis and economic evaluation for manufacturing hydroxyapatite nanoparticles from eggshell waste. *Int. J. Res. Appl. Technol.* **1**(1), 211–226 (2021)
- Koroleva, M.Y.; Karakatenko, E.Y.; Yurtov, E.V.: Synthesis of hydroxyapatite nanoparticles by controlled precipitation in the presence of sodium dodecyl sulfate. *Colloid J.* **82**(3), 275–283 (2020). <https://doi.org/10.1134/S1061933X20030059>



34. Xu, Z.; Qian, G.; Feng, M.: Using polyacrylamide to control particle size and synthesize porous nano hydroxyapatite. *Results Phys.* **16**, 102991 (2020)
35. Ungureanu, D.N.; Angelescu, N.; Tsakiris, V.; Marinescu, V.: Investigations regarding chemical synthesis of calcium hydroxyapatite. *Romanian J. Mater.* **42**(1), 52–60 (2012)
36. Elochukwu, H.; Gholami, R.; Dol, S.S.: An approach to improve the cuttings carrying capacity of nano silica-based muds. *J. Pet. Sci. Eng.* **152**, 210–216 (2017)
37. Wang, Y.J.; Chen, J.D.; Wei, K.; Zhang, S.H.; Wang, X.D.: Surfactant assisted synthesis of hydroxyapatite particles. *Mater. Lett.* **60**, 3227–3231 (2006)
38. Sabry, A.A.; Salih, N.A.: Synthetic properties of hydroxyapatite powder prepared from natural eggs shell. *J. Green Eng.* **10**(7), 3498–3507 (2020)
39. Oseh, J.O.; Norddin, M.N.A.M.; Ismail, I.; Duru, U.I.; Gbadamosi, A.O.; Agi, A.; Ngouangna, E.N.; Blkooor, S.O.; Yahya, M.N.; Risal, A.R.: Rheological and filtration control performance of water-based drilling muds at different temperatures and salt contaminants using surfactant-assisted novel nanohydroxyapatite. *Geoenergy Sci. Eng.* **228**, 1–18 (2023). <https://doi.org/10.1016/j.geoen.2023.211994>
40. API RP 13B-2: Recommended Practice for Field Formulation of Water-Based Drilling Fluids, 5th edn. API, Washington (2019)
41. API RP 13B-1: Recommended Practice for Field Testing Water-Based Drilling Fluids, 5th edn. API, Washington (2019)
42. Ngouangna, E.N.; Jaafar, M.D.; Mohd Norddin, M.N.A.; Agi, A.; Oseh, J.O.; Mamah, S.: Surface modification of nanoparticles to improve oil recovery mechanisms: a critical review of the methods, influencing Parameters, advances and prospects. *J. Mol. Liq.* **360**, 119502 (2022)
43. Merlo, A.; Maglione, R.; Piatti, C.: An innovative model for drilling fluid hydraulics. In: Paper SPE 29259 Presented at SPE Oil and Gas Conference, 20–22 March, Kuala Lumpur (1995)
44. Zamora, M.; Roy, S.; Slater, K.: Comparing a basic set of drilling fluid pressure-loss relationships to flow-loop and field data. In: Paper AADE-05-NTCE-27 Presented at the AADE National Technical Conference and Exhibition, 5–7 April, Houston, USA (2005)
45. Wang, J.; Chen, M.; Li, X.; Yin, X.; Zheng, W.: Effect of synthetic quadriopolymer on rheological and filtration properties of bentonite-free drilling fluid at high temperature. *Crystals* **12**, 257 (2022). <https://doi.org/10.3390/cryst12020257>
46. Chernikov, O.I.; Glagolev, R.V.; Zvyagina, T.I.: Thermostability of surfactants having various chemical structures. *J. Appl. Chem.* **56**(6), 1347–1349 (2019)
47. Córdova-Udaeta, M.; Kim, Y.; Yasukawa, K.; Kato, Y.; Fujita, T.; Dodbiba, G.: Study on the synthesis of hydroxyapatite under highly alkaline conditions. *Ind. Eng. Chem. Res.* **60**, 4385–4396 (2021)
48. Manafi, S.A.; Yazdani, B.; Rahimiopour, M.R.; Sadrnezhaad, S.K.; Amin, M.H.; Razavi, M.: Synthesis of nano-hydroxyapatite under a sonochemical/hydrothermal condition. *Biomed. Mater.* **3**(2), 025002 (2008). <https://doi.org/10.1088/1748-6041/3/2/025002>
49. Wei, Z.; Wang, M.; Li, Y.; An, Y.; Li, K.; Bo, K.; Guo, M.: Sodium alginate as an eco-friendly rheology modifier and salt-tolerant fluid loss additive in water-based drilling fluids. *RSC Adv.* **19**(46), 29852–29864 (2022). <https://doi.org/10.1039/d2ra04448j>
50. Lidén, A.; Naidjonoka, P.; Karna, N.K.; Theliander, H.: Structure of filter cakes during the electroassisted filtration of microfibrillated cellulose. *Ind. Eng. Chem. Res.* **61**(43), 16247–16256 (2022)
51. Yao, R.; Jiang, G.; Li, W.; Deng, T.; Zhang, H.: Effect of water-based drilling fluid components on filter cake structure. *Powder Technol.* **262**, 51–61 (2014)
52. Grover, I.S.; Singh, S.; Pal, B.: The preparation, surface structure, zeta potential, surface charge density and photocatalytic activity of TiO₂ nanostructures of different shapes. *Appl. Surf. Sci.* **280**, 366–372 (2013)

Springer Nature or its licensor (e.g. a society or other partner) holds exclusive rights to this article under a publishing agreement with the author(s) or other rightsholder(s); author self-archiving of the accepted manuscript version of this article is solely governed by the terms of such publishing agreement and applicable law.

